



## OPEN ACCESS

## EDITED BY

Juan Santos Echeandia,  
Spanish Institute of Oceanography  
(IEO), Spain

## REVIEWED BY

Aridane G. Gonzalez,  
University of Las Palmas de Gran  
Canaria, Spain  
Kristen Nicolle Buck,  
University of South Florida,  
United States  
Hajime Obata,  
The University of Tokyo, Japan

## \*CORRESPONDENCE

Francisco Delgadillo-Hinojosa  
✉ [fdelgadillo@uabc.edu.mx](mailto:fdelgadillo@uabc.edu.mx)

## SPECIALTY SECTION

This article was submitted to  
Marine Pollution,  
a section of the journal  
Frontiers in Marine Science

RECEIVED 04 September 2022

ACCEPTED 09 December 2022

PUBLISHED 06 January 2023

## CITATION

Félix-Bermúdez A,  
Delgadillo-Hinojosa F, Lares ML,  
Torres-Delgado EV, Huerta-Díaz MA,  
Tovar-Sanchez A and  
Camacho-Ibar VF (2023) Spatial  
variability of dissolved nickel is  
enhanced by mesoscale dynamics in  
the Gulf of Mexico.  
*Front. Mar. Sci.* 9:1036331.  
doi: 10.3389/fmars.2022.1036331

## COPYRIGHT

© 2023 Félix-Bermúdez,  
Delgadillo-Hinojosa, Lares,  
Torres-Delgado, Huerta-Díaz,  
Tovar-Sanchez and Camacho-Ibar. This  
is an open-access article distributed  
under the terms of the [Creative  
Commons Attribution License \(CC BY\)](https://creativecommons.org/licenses/by/4.0/).  
The use, distribution or reproduction  
in other forums is permitted, provided  
the original author(s) and the  
copyright owner(s) are credited and  
that the original publication in this  
journal is cited, in accordance with  
accepted academic practice. No use,  
distribution or reproduction is  
permitted which does not comply with  
these terms.

# Spatial variability of dissolved nickel is enhanced by mesoscale dynamics in the Gulf of Mexico

Armando Félix-Bermúdez<sup>1</sup>, Francisco Delgadillo-Hinojosa<sup>1\*</sup>,  
María Lucila Lares<sup>2</sup>, Eunise Vanessa Torres-Delgado<sup>1</sup>,  
Miguel Angel Huerta-Díaz<sup>1</sup>, Antonio Tovar-Sanchez<sup>3</sup>  
and Víctor Froylan Camacho-Ibar<sup>1</sup>

<sup>1</sup>Instituto de Investigaciones Oceanológicas, Universidad Autónoma de Baja California, Ensenada, Mexico, <sup>2</sup>Departamento de Oceanografía Biológica, División de Oceanología, Centro de Investigación Científica y de Educación Superior de Ensenada, Ensenada, Mexico, <sup>3</sup>Departamento de Ecología y Gestión Costera, Instituto de Ciencias Marinas de Andalucía ICMAN-CSIC, Puerto Real, Cadiz, Spain

The Gulf of Mexico (GoM) is one of the most dynamic marginal seas in the world owing to the intrusion of the Loop Current and the shedding of anticyclonic eddies (LCE) that travel westward across the Gulf. However, the impacts of these mesoscale dynamics on the supply and removal of bioessential trace metals in surface waters remain unclear. We study the impact of mesoscale eddies on the distribution of dissolved nickel (Ni), a biologically active element scarcely studied in the region. The vertical distribution of Ni was determined in the deep-water region of the GoM during summer of 2017, when two anticyclonic LCE (Quantum and Poseidon) were present. Nutrient-like profiles of Ni in the GoM resemble those from the Atlantic Ocean, but they showed high spatial variability within the first 1000 m, which was associated with the impact of mesoscale eddies. Similarly to subtropical gyres, macronutrients were almost depleted in surface waters, while Ni never fell below 1.51 nmol kg<sup>-1</sup>, suggesting low Ni lability or alternatively, slow biological uptake compared to that of macronutrients. In particular, lowest levels of Ni and macronutrients (PO<sub>4</sub> and NO<sub>3</sub>) were recorded in surface waters of the anticyclonic eddies and the Loop Current area. Anticyclonic LCEs deepened these Ni-poor waters pushing the Ni-rich core of Tropical Atlantic Central Water up to 600 m, whereas its shallowest position (up to 200 m) was recorded under cyclonic conditions in Campeche Bay. This eddy-induced vertical displacement of water masses also affected the integrated Ni and macronutrient concentrations in the upper 350 m but without modifying their stoichiometries. We suggest that a significant decrease in surface inventories of Ni and macronutrient in areas impacted by LCEs is a consequence of the trapping of the water within eddies, the biological uptake of Ni and macronutrients combined with their limited replenishment

from below, which likely affects autotrophic groups. In conclusion, the mesoscale dynamic permanently present in the GoM play an important role in modifying the vertical distribution of Ni and macronutrients as well as their availability in the upper water column of this marginal sea.

#### KEYWORDS

dissolved nickel, mesoscale eddies, loop current, Tropical Atlantic Central Water, Gulf of Mexico, macronutrients

## 1 Introduction

Nickel is an essential micronutrient for marine phytoplankton given that it plays a fundamental role in the transformation of urea to ammonium and consequently in the assimilation of alternate nitrogen sources for primary production (Price and Morel, 1991; Egleston and Morel, 2008; Dupont et al., 2010; Twining et al., 2012). Additionally, it is essential for the proper functioning of nitrogen-fixing enzymes and protects cyanobacteria and other marine microbes from reactive radicals produced by their own metabolisms (Ho, 2013; Glass and Dupont, 2017). Owing to its involvement in the biogeochemical cycle of organic matter, the vertical distribution of dissolved Ni in the ocean follows that of a nutrient, with minimum concentrations in the euphotic zone due to consumption by primary producers and a gradual increase in concentration with increasing depth due to the remineralization of sinking organic matter (Sclater et al., 1976; Bruland, 1980; Saager et al., 1997; Lemaitre et al., 2022). Thus, the vertical distribution of Ni in the ocean presents a positive, nearly linear relationship with the corresponding distributions of macronutrients (e.g.,  $\text{PO}_4$  and  $\text{SiO}_4$ ) and bio-essential metals (e.g., Cd, Fe, and Zn; Bruland, 1980; Yeats and Campbell, 1983; Danielsson et al., 1985; Cloete et al., 2019; Middag et al., 2020).

The vertical distributions of Ni in the Atlantic and Pacific oceans have a similar shape; however, Ni concentrations are higher in deep Pacific waters relative to deep Atlantic waters due to accumulation of remineralized Ni along the path of deep-water circulation (Boyle et al., 1981; Bruland and Franks, 1983; Glass and Dupont, 2017). In contrast, the surface Ni concentrations in both oceans rarely fall below  $1.5 \text{ nmol kg}^{-1}$ , and remain at values close to  $2 \text{ nmol kg}^{-1}$  (Yeats and Campbell, 1983; Kremling, 1985; Yeats et al., 1995; Saager et al., 1997; Bowie et al., 2002; Middag et al., 2020; Lemaitre et al., 2022), which is contrary to other bioactive elements that are almost depleted in surface waters (e.g., Fe; Conway et al., 2018; Sedwick et al., 2020). Some authors have suggested that this excess concentration represents a pool of Ni apparently “non-accessible” for the phytoplankton that depends on urea or other alternate sources of nitrogen in oligotrophic environments (Sunda, 1989; Mackey et al., 2002). This

argument has been supported by the fact that Ni is bound by organic multidentate chelators (Wen et al., 2006; Boiteau et al., 2016), which limits its bioavailability and, consequently, affects the phytoplankton growth (Dupont et al., 2010; Morel et al., 2014; Archer et al., 2020; Middag et al., 2020). However, as an alternative explanation for the low lability of Ni in surface waters, a recent study experimentally demonstrated that most of the dissolved Ni is chemically and biologically available (John et al., 2022). The authors tested the Ni bioavailability by culturing phytoplankton in an oligotrophic seawater media collected in the North Pacific Subtropical Gyre and amended with macronutrients and Fe. Their results suggest that the slow biological uptake of Ni becomes limited by the availability of the quickly consumed macronutrients, explaining the surface  $\sim 2 \text{ nM}$  Ni left over present in oligotrophic gyres.

Nickel in Atlantic surface waters is supplied through atmospheric deposition (Jickells et al., 2016) and, to a lesser extent, fluvial inputs from the Amazon and African rivers (Tovar-Sanchez et al., 2006; Tovar-Sanchez and Sañudo-Wilhelmy, 2011). Besides, the vertical distributions of Ni (and other bioactive trace metals) in marginal seas surrounding the Atlantic often contrast with those recorded in the open ocean. For example, the maximum Ni concentrations in the surface waters of the Mediterranean Sea are high (up to  $\sim 4 \text{ nmol kg}^{-1}$ ) due to both atmospheric and fluvial inputs (Saager et al., 1993; Morley et al., 1997; Zeri and Voutsinou-Taliadouri, 2003; Middag et al., 2022). Ni enrichment relative to the Ni levels in adjacent open ocean waters have also been observed in other marginal seas of the world, as the Gulf of California (Domínguez-Rosas, 2008), the Baltic Sea (Kremling, 1983), the Black Sea (Lewis and Landing, 1992) and the Yellow Sea (Zhang et al., 2022). However, even in Ni-rich systems such as these, Ni addition has been found to stimulate phytoplankton growth (e.g., Dupont et al., 2010), which reveals the complexity of the interactions between Ni and biological activity, and thus highlights the necessity to study the spatial distribution of this element and the factors that affect its availability to primary producers.

The Gulf of Mexico (GoM) is considered one of the most dynamic marginal seas in the world. The physical dynamics that

determine the distributions and mixing of the water masses within the Gulf are associated with the Loop Current System (LC; Kuznetsov et al., 2002; Oey et al., 2005). Upon entering the Gulf, the LC generates large anticyclonic mesoscale eddies with diameters measuring hundreds of kilometers and lifetimes spanning up to 17 months (Oey et al., 2005, and references therein; Meunier et al., 2018). These eddies can travel across the Gulf from east to west over the course of a few months and influence the vertical distributions of most water masses present in the GoM (Meunier et al., 2018; Sosa-Gutiérrez et al., 2020; Valencia-Gasti et al., 2022). The biogeochemical characteristics of macro and micronutrient concentrations (e.g., Ni) of the water masses within the GoM differ, with Caribbean Surface Water (CSW) generally considered to be the poorest (Pinedo-Gonzalez et al., 2015) and the deep-water masses of polar and subpolar origins generally considered to be the richest (Bowie et al., 2002; Middag et al., 2020). During summer, the mixed layer of the Gulf is shallow, and strong water-column stratification limits vertical mixing (Portela et al., 2018). Under these conditions, mesoscale eddies are the main factors controlling the vertical displacement of the water masses and its chemical composition. While cyclonic eddies produce an upward flux of nutrient-rich subsurface waters to the euphotic zone, anticyclonic eddies produce the downwelling of nutrient-poor waters to deeper layers (McGillicuddy, 2016). Hence, these mesoscale eddies are able to control the flux and availability of bioessential elements for primary producers that inhabit the surface waters of the GoM. In fact, it has recently been demonstrated that mesoscale eddies can modulate the inorganic nitrogen stock in the first 200 m under conditions of high stratification, which provides compelling evidence of the impacts of mesoscale dynamics on the euphotic zone of the GoM (Lee-Sánchez et al., 2022; Velásquez-Aristizábal et al., 2022). Thus, given their capabilities to generate mixing and vertical fluxes, mesoscale eddies should potentially have a strong control over the supply of Ni (and other elements with nutrient-like distributions) to surface waters and, consequently, on its availability to primary producers in the GoM.

In addition to the eddy-driven supply of Ni, the GoM is also influenced by fluvial inputs from the Mississippi-Atchafalaya system (Wen et al., 2011; Joung et al., 2019) and Mexican rivers (Martínez-López and Zavala-Hidalgo, 2009; González-Ramírez and Parés-Sierra, 2019), as well as the atmospheric dust supply from the Sahara Desert (Lenes et al., 2012; Hayes et al., 2022). These pathways could represent important sources of Ni to the Gulf. Besides, during the warm, stratified, and oligotrophic conditions of summertime, the phytoplankton biomass of surface waters is dominated by *Prochlorococcus* sp. (Linacre et al., 2019), a photosynthetic cyanobacteria that stands out for its high physiological demand for Ni (Price and Morel, 1991; Palenik et al., 2003). Likewise, a high abundance of nitrogen-fixing cyanobacteria (e.g., *Trichodesmium* spp.) could also be expected in offshore surface waters during summer conditions

(Hernández-Sánchez et al., 2022), as has been reported for shelf waters of the northern Gulf (e.g., Mulholland et al., 2006; Holl et al., 2007). Thus, the predominance of *Prochlorococcus* sp. coupled with an increase in the presence of diazotrophic groups characterized by their high rates of Ni consumption (Ho, 2013), could increase the demand for this element in the Gulf. All these characteristics make the GoM a unique site to study the biogeochemical behavior of dissolved Ni and other bioessential elements that could limit primary production. However, to the best of our knowledge, information on the spatiotemporal variation of dissolved Ni in the deep-water region of this marginal sea is still scarce (Boyle et al., 1984; Joung and Shiller, 2013; Hayes et al., 2019, and references therein; Mellett and Buck, 2020).

Therefore, the objectives of this study were to: 1) study the spatial distribution of Ni in the deep-water region of the Mexican portion of the GoM ( $\leq 25^\circ$  N) during summer, 2) compare the vertical distribution of Ni with that of the western Atlantic Ocean, 3) assess the influence of mesoscale physical dynamics on the spatial distribution of Ni, 4) examine the Ni relationship with macronutrients, and 5) evaluate the impact of mesoscale eddies on the stock of Ni in the surface layer of the GoM and its biogeochemical implications. We found that the vertical distribution of Ni in the GoM shows oceanographic consistency with the typical distribution of this element in the Atlantic Ocean, although it exhibits great spatial variability due to the influence of mesoscale eddies in the Gulf. We show that mesoscale eddy dynamics are able to decrease the Ni and macronutrient inventories in the surface waters of the GoM, which likely impacts the activity of primary producers.

## 2 Materials and methods

### 2.1 Study area

The GoM is one of the most dynamic marginal seas on the planet and the second largest marginal sea in the tropical-subtropical portion of the Atlantic Ocean. The Gulf has a total area of  $\sim 1.5 \times 10^6$  km<sup>2</sup>, an average depth of 1615 m and is shaped like the letter G (Figure 1A; Turner and Rabalais, 2019). The GoM is considered an evaporative basin, as evaporation exceeds precipitation by more than 1 m yr<sup>-1</sup>, which results in net heat gain (Tomczak and Godfrey, 2003). This marginal sea is occupied by water masses of tropical-subtropical origin at the surface and by water masses of polar-subpolar origin at greater depths (Portela et al., 2018; Valencia-Gasti et al., 2022). Before entering the GoM, these water masses pass through the Caribbean Sea, a deep marginal sea that communicates with the Atlantic Ocean through three narrow and deep passages ( $\sim 1500$  m). After crossing the Caribbean Sea, the Atlantic and Caribbean water masses enter the GoM through the Yucatan Channel ( $\sim 196$  km wide and 2000 m deep). The net

flow of water from the Caribbean Sea into the GoM ranges from 23.0 to 27.6 Sv ( $1 \text{ Sv} = 10^6 \text{ m}^3 \text{ s}^{-1}$ ; [Badan et al., 2005](#); [Candela et al., 2019](#)). In the first 1000 m, water flow is driven by the LC ([Figures 1A, B](#); [Kuznetsov et al., 2002](#); [Oey et al., 2005](#)), while the physical dynamics of the Gulf in deeper waters are dominated by currents produced by Rossby waves that follow the topography and by the eddies that emerge from these currents ([Furey et al., 2018](#)).

The LC reaches maximum speeds of  $2.5 \text{ m s}^{-1}$  ([Athié et al., 2012](#)) and can extend northward into the GoM up to  $\sim 25^\circ \text{ N}$ , after which the LC exits the system through the Florida Strait ([Figures 1A, B](#); [Kuznetsov et al., 2002](#); [Oey et al., 2005](#)). This current is responsible for the shedding of anticyclonic eddies, which are large mesoscale structures 200–350 km in diameter with life spans between 3 and 17 months ([Elliott, 1982](#); [Biggs et al., 1996](#); [Oey et al., 2005](#)). Once detached from the LC, these anticyclonic eddies travel westward (see gray arrow in [Figure 1A](#)) and their vertical influence can extend up to 1000 m depth ([Meunier et al., 2018](#)). In general, these mesoscale structures are responsible for much of the physical dynamics at the surface inside the Gulf, while diurnal tidal

forcing plays a much smaller role (tidal amplitudes are low and range from 11–17 cm; [Kantha, 2005](#)). It should be noted that LC anticyclonic eddies strongly impact the chemical and biological characteristics of the surface waters of the GoM given that they introduce warm and nutrient-depleted Caribbean waters and consequently affect primary productivity (e.g., [Biggs, 1992](#); [Linacre et al., 2015](#); [Lee-Sánchez et al., 2022](#)). On the contrary, cyclonic eddies, which develop as counterparts to the anticyclonic eddies ([Oey et al., 2005](#)), can overcome the thermal barrier created by highly stratified surface waters during the warm months of summer ([Portela et al., 2018](#)). Consequently, cyclonic eddies promote the flux of subsurface water to the euphotic zone, which provides essential elements for primary producers ([Durán-Campos et al., 2017](#)). In addition, all the rivers that flow into the Mexican portion of the GoM, including the Grijalva-Usumacinta, Pánuco, and Río Grande, also bring metals and nutrients into the Gulf ([Figure 1A](#)). Finally, atmospheric dust from the Sahara Desert that travels high across the Atlantic and eventually settles in the GoM, could also be a source of nutrients and metals to the surface waters (e.g., [Lenes et al., 2012](#); [Hayes et al., 2022](#)).

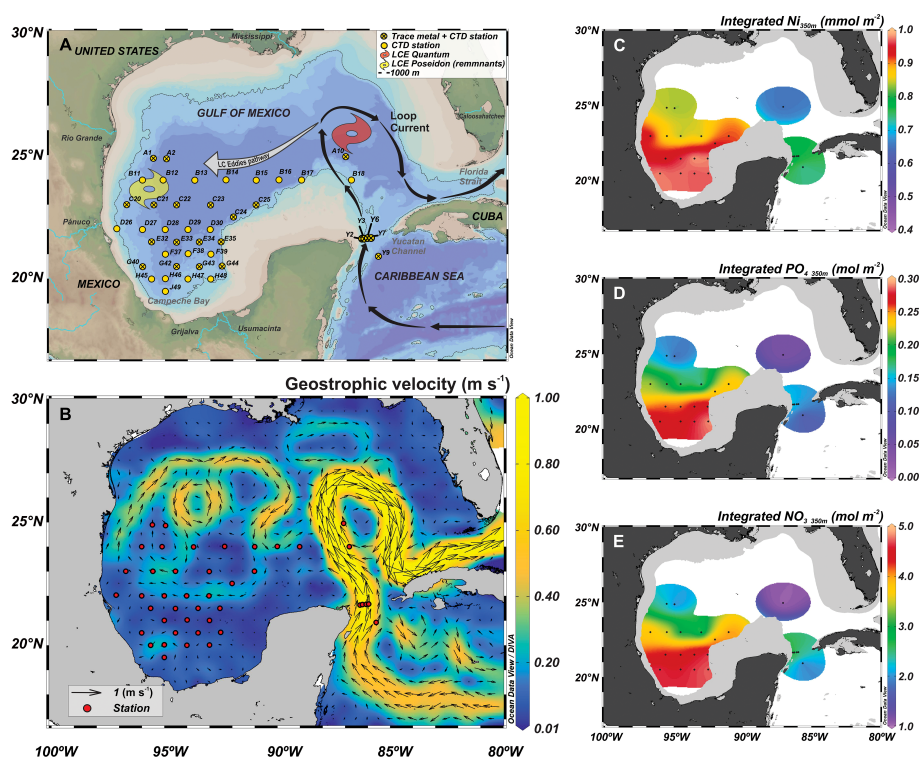


FIGURE 1

(A) Map of the Gulf of Mexico and sampling stations during the XIXIMI-6 cruise carried out in the summer of 2017 (August 19 to September 8). (B) Mean satellite-derived geostrophic velocity field during the cruise period. Mapping of the integrated concentration of (C) dissolved Ni, (D) phosphate ( $\text{PO}_4$ ) and (E) nitrate plus nitrite ( $\text{NO}_3$ ) in the first 350 m of the water column during the XIXIMI-6 cruise. The big gray arrow shown in panel (A) indicates the typical pathway and transport direction of the loop current eddies (LCE). The location of hydrographic sampling stations where the CTD casts were made are indicated by yellow and red circles in panels (A, B), respectively. Water samples for dissolved Ni and macronutrient analysis were also collected at stations with crossed yellow circles. This figure was made using Ocean Data View ([Schlitzer, 2021](#)).

## 2.2 Cleaning procedures

All materials used for sample collection at sea and in laboratory analysis were cleaned following the rigorous ultra-clean protocols designed for collecting and measuring trace metals in sea water (Bruland et al., 1979; Delgadillo-Hinojosa et al., 2006; Delgadillo-Hinojosa et al., 2015; Cutter et al., 2017; Hernández-Candelario et al., 2019; Félix-Bermúdez et al., 2020). Briefly, the plastic (e.g., low density polyethylene bottles and pipette tips) and Teflon (e.g., tubing, extraction funnels, and bottles) materials were washed with a phosphate-free alkaline detergent (3%; Micro-90<sup>®</sup>), rinsed with plenty of distilled water ( $\geq 10.0$  M $\Omega$  cm), and submerged for one week in the Micro-90<sup>®</sup> solution. Then, the materials were rinsed with deionized water (DIW, 18.2 M $\Omega$  cm) until there were no traces of detergent. After which, the materials were kept for a month in a 3 M HCl solution (reagent grade, J.T. Baker<sup>®</sup>). Over time, the materials were removed from the acid solution, rinsed 4x with DIW and then soaked for a week in a 1 M HNO<sub>3</sub> solution (Omnitrace grade) to eliminate any traces of persistent contamination. Finally, the materials were rinsed 5x with DIW and dried inside a laminar flow hood installed in a Class-100 clean laboratory. The low-density polyethylene bottles (LDPE) used for the collection of seawater samples were previously filled with a 0.01 M HNO<sub>3</sub> Ultrex<sup>®</sup> solution (J.T. Baker<sup>®</sup>), double-bagged, and transported in closed plastic buckets to the field. In the case of LDPE bottles for macronutrient analysis, the steps of using HNO<sub>3</sub> were omitted. The Niskin-X bottles (General Oceanic Inc., Miami, FL, USA) used for seawater sampling were washed using the Micro-90<sup>®</sup> solution and distilled water. The bottles remained filled with the Micro-90<sup>®</sup> solution for one day. Subsequently, the bottles were abundantly rinsed with DIW and filled with a 3 M HCl solution (analytical grade, J.T. Baker<sup>®</sup>) for one day. Finally, the acid solution was discarded through the drain valve, and the bottles were abundantly rinsed with DIW, closed, and stored in double plastic bags until use during the cruise.

## 2.3 Sample collection

Seawater samples were collected during the XIXIMI-6 campaign (August 19 to September 8, 2017) on board the R/V Justo Sierra. In all, 43 hydrographic stations in the deep-water region of the GoM were sampled (Figure 1A). At each hydrographic station, vertical profiles of temperature, salinity and dissolved oxygen were recorded using a SeaBird CTD (SeaBird Scientific, Bellevue, WA, USA). Temperature and salinity data were converted to conservative temperature (T) and absolute salinity (S<sub>A</sub>) following TEOS-10 equations (IOC et al., 2010). The CTD data had a spatial resolution of 1 m, and each cast covered a depth range of 2 to 3730 m depending on the bathymetry of each station. A total of 22 oceanographic stations and up to 12 depth levels per station were selected to collect

samples for macronutrients and dissolved Ni analysis (total of 160 water samples). Water samples were collected using acid-cleaned 20-L Teflon coated Niskin-X bottles installed in an epoxy painted oceanographic rosette. Seawater for Ni analysis was pumped from the Niskin-X bottles into a shipboard Class-100 clean room using a peristaltic pump while being filtered through an acid-cleaned 0.2  $\mu$ m Supor AcroPak 200 filter (Pall Corporation, New York, NY, USA) and C-Flex hose that had been previously washed with acid and DIW. Filtered seawater was recovered in acid-cleaned LDPE bottles and acidified to pH < 2 with 1 mL of HNO<sub>3</sub> Ultrex<sup>®</sup> (J.T. Baker<sup>®</sup>). The LDPE bottles were stored in two Ziplok plastic bags, placed inside buckets with airtight lids, and transported to an ultra-clean laboratory on land for analysis (Delgadillo-Hinojosa et al., 2006; Segovia-Zavala et al., 2010; Hernández-Candelario et al., 2019; Félix-Bermúdez et al., 2020). Samples for inorganic phosphate (PO<sub>4</sub>) and nitrate plus nitrite (NO<sub>3</sub>+NO<sub>2</sub>; hereafter NO<sub>3</sub>) analysis were collected directly from the Niskin-X bottles, filtered through pre-combusted Whatman GF/F filters (only for samples in the upper 250 m) and stored in LDPE bottles at -20°C until chemical analysis.

## 2.4 Analysis of macronutrients (PO<sub>4</sub> and NO<sub>3</sub>)

Concentrations of PO<sub>4</sub> and NO<sub>3</sub> in water samples were determined using wet chemical colorimetry (Armstrong et al., 1967; Gordon et al., 1993; Lee-Sánchez et al., 2022) with an AA3-HR segmented flow autoanalyzer (Seal Analytical, Fareham, UK). Analytical precision and accuracy were obtained by repeated measurements of the SCOR-JAMSTEC certified reference material (Lots CD and CC; Kanzo Co. Ltd., Osaka, Japan). Detection limits for PO<sub>4</sub> and NO<sub>3</sub> were 0.02  $\mu$ mol kg<sup>-1</sup> and 0.02  $\mu$ mol kg<sup>-1</sup>, respectively.

## 2.5 Analysis of dissolved Ni

To minimize the risk of contamination, handling and processing of seawater samples were carried out in an ultra-clean laboratory (Class-100) on land. Nickel in the filtered seawater samples was pre-concentrated using the classic organic extraction method (Bruland et al., 1979; Segovia-Zavala et al., 2010; Tovar-Sánchez, 2012) with an additional back-extraction step (Komjarova and Blust, 2006; Félix-Bermúdez et al., 2020). In general, this method is based on the chelation of dissolved metals with a mix of ammonium 1-pyrrolidinedithiocarbamate (APDC; 99% purity) and diethylammonium diethyldithiocarbamate (DDDC; 97% purity), a double extraction in chloroform (HPLC grade, washed with DIW) of the organic complex, and a back-extraction in a diluted solution of HNO<sub>3</sub> Ultrex<sup>®</sup> (J.T. Baker<sup>®</sup>). Briefly, the sample of acidified seawater was weighed (~ 250 g) and placed in a 500-mL Teflon separatory funnel. Then, the samples were buffered at pH 4.5 by the addition of

ammonium acetate (1 M), and 1 mL of the APDC/DDDC mixture (ratio of 1.1%) was added. Subsequently, a double extraction was performed by adding 8 and 6 mL of chloroform during the first and second extractions, respectively. After each extraction, chloroform was recovered in a 100-mL Teflon separatory funnel. The back-extraction was conducted by adding 100  $\mu\text{L}$  of  $\text{HNO}_3$  (Ultrex<sup>®</sup>) and 3 mL of DIW to the chloroform recovered in the separatory funnel. The mixture was allowed to stand for 5 min to separate the phases, after which the chloroform phase was discarded. The supernatant was recovered in acid-cleaned 8-mL LDPE bottles and stored at room temperature until analysis. The Ni concentration was quantified by inductively coupled plasma mass spectrometry (ICP-MS; ICAP-Q; Thermo-Fisher Scientific, Waltham, MA, USA) using external standards and rhodium as the internal standard. Procedural blanks were prepared using DIW (18.2 M $\Omega$  cm) and treated like the samples during pre-concentration and analysis. The analytical quality control included analysis of procedural blanks and certified reference material NASS-7 (National Research Council of Canada). Ni levels in procedural blanks ( $0.040 \pm 0.002 \text{ nmol kg}^{-1}$ ) were always below the detection limit of the method ( $0.15 \pm 0.09 \text{ nmol kg}^{-1}$ ; calculated as three times the standard deviation of the blanks). The measured Ni concentrations in NASS-7 ( $4.06 \pm 0.01 \text{ nmol kg}^{-1}$ ) compared well with the certified value ( $4.14 \pm 0.31 \text{ nmol kg}^{-1}$ ) with an average recovery of  $98.0 \pm 1.7\%$  ( $n = 5$ ).

## 2.6 Satellite data

Images of absolute dynamic topography (ADT) and geostrophic velocity were obtained from the altimetry estimates available for download on the AVISO website (<https://las.aviso.altimetry.fr>). Daily MODIS/Aqua images (Standard mapped and 4 km resolution) of sea surface temperature (SST) and chlorophyll-a (Chl-a) were downloaded from the Ocean Color website of the National Aeronautics and Space Administration (NASA; <https://oceancolor.gsfc.nasa.gov/>). Satellite-based net primary production (NPP) images were retrieved from the Oregon State University website (<http://science.oregonstate.edu/ocean.productivity>); the carbon-based primary productivity model (CbPM) at a resolution of 9 km was selected. Image processing was carried out using SeaDAS v. 7.5.1. (NASA).

## 2.7 Statistical analysis

The normality of the data distribution was evaluated with the Shapiro-Wilk test. Analyses of differences between two groups were conducted with student t-tests or Mann-Whitney rank sum tests for parametric and non-parametric distributions, respectively. Pearson correlation analyses were used to evaluate relationships between pairs of variables. Results were considered significant at  $\alpha = 0.05$ , and all analyses were conducted with Statistica v. 10 (StatSoft, Tulsa, OK, USA).

## 3 Results

### 3.1 Satellite-derived absolute dynamic topography and geostrophic velocities

The XIXIMI-6 campaign (summer 2017) took place four months after the large LC eddy (hereafter LCE) Poseidon dissipated in the northwestern portion of the GoM and two months before eddy Quantum separated from the LC in the northeastern GoM (<http://www.horizonmarine.com>). This oceanographic context resulted in contrasting ADT and geostrophic velocity conditions in the Gulf (Figures 1B, 2A) and allowed for three regions to be identified: 1) a highly dynamic region in the northeastern GoM ( $\text{ADT} > 0.78 \text{ m}$  and geostrophic velocity  $> 1 \text{ m s}^{-1}$ ); 2) a region of moderate mesoscale dynamics in the northwestern GoM ( $0.55 \text{ m} < \text{ADT} < 0.78 \text{ m}$ ;  $0.5 \text{ m s}^{-1} < \text{geostrophic velocity} < 1 \text{ m s}^{-1}$ ); and 3) the weak mesoscale dynamic region in the southern GoM ( $\text{ADT} < 0.55 \text{ m}$ ; geostrophic velocity  $< 0.5 \text{ m s}^{-1}$ ).

In the high mesoscale dynamics region, the intrusion of the LC through the Yucatan Channel was the most notable surface circulation feature (Figure 1B). The LC was limited to the eastern portion of the GoM ( $85\text{--}88^\circ \text{ W}$ ; stations Y2–Y9 and A10), and its influence to the north extended to  $27^\circ \text{ N}$ . The northernmost extension of the LC was associated with the anticyclonic LCE Quantum (diameter of  $\sim 300 \text{ km}$ ), whose core was located in the vicinity of station A10 (Figure 2A). In the case of the moderate dynamics region, an U-shaped mesoscale structure was detected in the northwestern GoM (Figure 1B), which was formed by two elongated anticyclonic eddies separated by a circular cyclonic eddy (Figure 2A). These anticyclonic eddies were remnants of the LCE Poseidon and had the greatest influence over stations A1, A2, and B11–B13. The geostrophic velocities and ADT values in this region were  $\sim 50\%$  lower than those estimated in the region influenced by the LC and its eddy. Finally, in stark contrast to the other two regions, the lowest geostrophic velocities ( $< 0.15 \text{ m s}^{-1}$ ; Figure 1B) and ADT values ( $< 0.3 \text{ m}$ ; Figure 2A) were observed in Campeche Bay within the domain of a semi-permanent cyclonic eddy, which were indicative of less energetic mesoscale dynamics present in that area during the XIXIMI-6 campaign.

### 3.2 Satellite-derived temperature, chlorophyll-a, and net primary productivity

The three regions exhibited distinct SST, Chl-a, and NPP values (Figures 2B–D). For example, the LC in the Yucatan Channel and eddy Quantum in the northeastern GoM were characterized by warm waters, low phytoplankton biomass ( $\sim 0.05 \text{ mg m}^{-3}$ ) and low NPP ( $\sim 0.29 \text{ g C m}^{-2} \text{ d}^{-1}$ ; Figures 2B–D). Similarly, the remnants of the anticyclonic LCE Poseidon were also distinguishable by warm

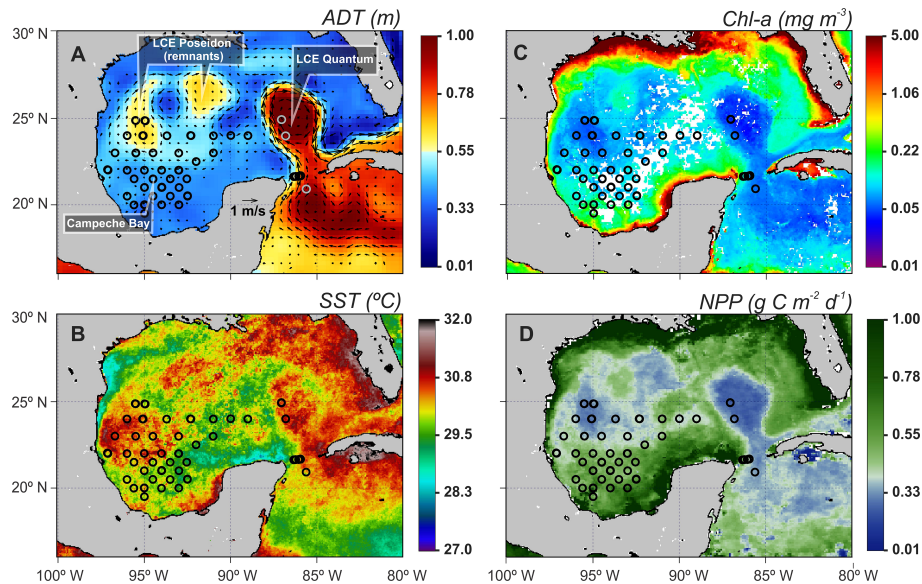


FIGURE 2

Satellite-derived images of (A) absolute dynamic topography (ADT; color scale) and geostrophic velocity (arrows), (B) sea surface temperature (SST), (C) chlorophyll a (Chl-a), and (D) net primary production (NPP) during the XIXIMI-6 cruise. Each panel represents a 21-day composite image that spans from August 19 to September 8, 2017. The locations of anticyclonic Loop Current eddies (LCE) are indicated in (A).

and oligotrophic waters with Chl-a values of  $\sim 0.08 \text{ mg m}^{-3}$  and NPP values of  $\sim 0.32 \text{ g C m}^{-2} \text{ d}^{-1}$  (Figures 2B–D). In contrast to the other two regions, Campeche Bay exhibited slightly colder waters and higher Chl-a (maximum of  $0.6 \text{ mg m}^{-3}$ ) and NPP (maximum of  $0.69 \text{ g C m}^{-2} \text{ d}^{-1}$ ) values (Figures 2B–D).

### 3.3 Spatial distributions of water masses

According to the hydrographic classification for the central and western portions of the GoM (Portela et al., 2018), six water masses were detected during the XIXIMI-6 campaign (Table 1; Figure 3). The sectional distribution of absolute salinity ( $S_A$ ) also shows that above 200 m depth, the remnant of Caribbean Surface Water (CSWr) and North Atlantic Subtropical Underwater (NASUW) dominated the region influenced by the LC and LCE Quantum (stations Y9 and A10), whereas CSWr and Gulf Common Water (GCW) dominated stations in the northwestern (A1–A2) and southwestern (G40) portions of the GoM (Figure 3A). Below 200 m depth, Tropical Atlantic Central Water (TACW) formed a layer  $\sim 400 \text{ m}$  thick (Figures 3A, B). The influence of mesoscale eddies on the vertical position of each water mass was evident in the first 600 m of the water column, with a clear deepening of the isohalines in areas under the influence of anticyclonic eddies (LCE Quantum and the remnants of the LCE Poseidon) and an elevation of the isohalines in the region influenced by the semi-permanent cyclonic eddy of Campeche Bay (Figure 3A).

On the other hand, the deep waters of the GoM were composed by Antarctic Intermediate Water (AAIW) and North Atlantic Deep Water (NADW; Figure 3B). AAIW exhibited a well-defined distribution throughout the three regions of the GoM and maintained a layer  $\sim 500 \text{ m}$  thick that was found within the depth range of 600–1100 m (Figure 3B). Finally, NADW was the dominant water mass at depths  $> 1000 \text{ m}$  (Figure 3B). The influence of mesoscale eddies on the vertical positions of deep water masses in the GoM was much less evident than with shallower water masses (Figure 3B).

### 3.4 Spatial distribution of dissolved Ni

The vertical distribution of Ni in the GoM was oceanographically consistent with a nutrient-type profile in the global ocean; with low surface values ( $10 \text{ m}$ :  $1.95 \pm 0.15 \text{ nmol kg}^{-1}$ ) that gradually increased to maxima located between 600 ( $4.28 \pm 0.31 \text{ nmol kg}^{-1}$ ) and 1000 m depth ( $4.25 \pm 0.28 \text{ nmol kg}^{-1}$ ), to finally show a slight decrement and to stabilize in deep water ( $2500 \text{ m}$ :  $4.08 \pm 0.44 \text{ nmol kg}^{-1}$ ; Figures 4A–C). However, the distribution of Ni exhibited high vertical and horizontal variability throughout the GoM (Figures 4A, B), which was associated with changes in the spatial distributions of the water masses inside the Gulf (Figures 3A, B).

Table 1 shows the concentration of Ni for each water mass in each of the three hydrographic regions identified during the XIXIMI-6 campaign. In the first 100 m of the water column,

**TABLE 1** Average concentration of dissolved Ni ( $\pm$  standard deviation) in the water masses detected in three contrasting regions of the Gulf of Mexico in terms of mesoscale dynamics during the XIXIMI-6 cruise.

Water mass	$S_A$ (g kg <sup>-1</sup> )	T (°C)	Dissolved Ni (nmol kg <sup>-1</sup> ) [Water depth (m)]				
			Gulf of Mexico			Atlantic Ocean	
			SPC-CB	LCRr-Poseidon	LC+LCE-Quantum	Sargasso Sea	Tropical Atlantic
CSWr	36.35-36.70	22.0-28.0	2.04 $\pm$ 0.11 [64 $\pm$ 19]	2.03 $\pm$ 0.21 [107 $\pm$ 37]	1.71 $\pm$ 0.11 [89 $\pm$ 28]	2.04 $\pm$ 0.02 [19 $\pm$ 7]	1.97 $\pm$ 0.04 [72 $\pm$ 23]
GCW	36.55-36.80	20.0-22.5	2.16 $\pm$ 0.21 [80 $\pm$ 14]	2.20 $\pm$ 0.28 [151]	— —	2.03 [27 $\pm$ 5]	— —
NASUW	36.80-37.20	20.0-25.0	— —	— —	1.96 $\pm$ 0.03 [189 $\pm$ 49]	2.05 $\pm$ 0.08 [97 $\pm$ 50]	2.16 $\pm$ 0.05 [175 $\pm$ 26]
TACW	35.10-36.60	8.0-20.0	3.25 $\pm$ 0.52 [298 $\pm$ 138]	3.61 $\pm$ 0.64 [468 $\pm$ 114]	3.47 $\pm$ 0.61 [486 $\pm$ 142]	3.15 $\pm$ 0.70 [669 $\pm$ 140]	3.38 $\pm$ 0.54 [434 $\pm$ 139]
TACWc	35.25-35.90	9.0-13.0	3.68 $\pm$ 0.36 [409 $\pm$ 25]	3.67 $\pm$ 0.50 [458 $\pm$ 41]	3.52 $\pm$ 0.46 [559 $\pm$ 105]	3.95 $\pm$ 0.14 [755 $\pm$ 65]	3.85 $\pm$ 0.33 [484 $\pm$ 111]
AAIW	<35.3	5.0-6.5	4.20 $\pm$ 0.43 [10001 $\pm$ 1]	4.35 $\pm$ 0.29 [1002 $\pm$ 2]	3.84 $\pm$ 0.20 [977 $\pm$ 32]	4.19 $\pm$ 0.25 [1097 $\pm$ 72]	5.11 $\pm$ 0.17 [891 $\pm$ 115]
NADW	35.13-35.16	<4.5	4.20 $\pm$ 0.25 [1925 $\pm$ 538]	4.08 $\pm$ 0.39 [2125 $\pm$ 249]	3.80 $\pm$ 0.16 [2399 $\pm$ 483]	4.04 $\pm$ 0.22 [2035 $\pm$ 288]	3.95 $\pm$ 0.05 [2014 $\pm$ 175]

1) Semi-permanent cyclone in Campeche Bay (SPC-CB: stations E32-E35, G40, G42-G44), 2) remnants of Loop Current eddy Poseidon (LCRr-Poseidon: stations A1, A2, C20-C23) and 3) Loop Current (LC) + Loop Current eddy Quantum (LCR-Quantum: stations Y2, Y3, Y6, Y7, Y9, A10). For comparison, the average concentrations of Ni in the North Atlantic, specifically in the Sargasso Sea (GA02: E21-E25) and Tropical North Atlantic (GA02: E30-E34) from the GEOTRACES GA02 transect, are included (Schlitzer et al., 2018; Middag et al., 2020). The definition of water masses was based on the classification proposed by Portela et al. (2018) and the ranges of conservative temperature (T) and absolute salinity ( $S_A$ ) correspond to those measured during XIXIMI-6. The average depth where each water mass was detected is shown in square brackets. Abbreviations for water masses: CSWr, Caribbean Surface Water remnant; GCW, Gulf Common Water; NASUW, North Atlantic Subtropical Underwater; TACWc, Tropical Atlantic Central Water core; AAIW, Antarctic Intermediate Water; and NADW, North Atlantic Deep Water.

which was dominated by CSWr, the average Ni concentration in the LC area ( $1.71 \pm 0.11$  nmol kg<sup>-1</sup>) was significantly lower ( $p < 0.05$ ) than that of the region of the remnants of LCE Poseidon ( $2.03 \pm 0.21$  nmol kg<sup>-1</sup>) and the region of the semi-permanent cyclonic eddy in Campeche Bay ( $2.04 \pm 0.11$  nmol kg<sup>-1</sup>; Table 1 and Figure 4A). The Ni-depleted portion of CSWr was detected up to 91° W, from station Y9 outside the Yucatan Channel to station C25 (~ 1050 km; Figure 4A). This spatial variation reflects a slight Ni enrichment in the CSWr inside the GoM ( $\Delta Ni = 0.33$  nmol kg<sup>-1</sup>), which was not observed in any other water mass (Table 1). Below this water mass, NASUW exhibited the second lowest average concentration of Ni ( $1.96 \pm 0.03$  nmol kg<sup>-1</sup>) during the XIXIMI-6 campaign (Table 1).

Inside the Gulf, and particularly in the regions influenced by remnants of the anticyclonic LCE Poseidon and semi-permanent cyclonic eddy of Campeche Bay, a slight recovery of Ni levels was observed in GCW when compared to those observed in CSWr (Table 1; Figure 4A). However, below 200 m and up to 600 m depth, TACW showed a remarkable recovery in Ni levels (Figure 4A), with average concentrations ranging from  $3.25 \pm 0.52$  nmol kg<sup>-1</sup> to  $3.61 \pm 0.64$  nmol kg<sup>-1</sup> (Table 1). If we consider this result and the existence of intense vertical pumping conditions, TACW is the subsurface water mass with the greatest potential to act as a source of Ni to the euphotic zone in the GoM. In fact, Figure 4A shows a gradual ascent

of TACW waters (and its high content of Ni) from the Caribbean (Y9) to the Campeche Bay (G40). Below 600 m, AAIW and NADW were found to have average Ni concentrations ranging from  $3.80 \pm 0.16$  to  $4.20 \pm 0.43$  nmol kg<sup>-1</sup> (Figure 4B; Table 1). AAIW showed some of the highest Ni values; however, they were not significantly different from those of NADW ( $p > 0.050$ ; Figure 4B).

### 3.5 Spatial distribution of PO<sub>4</sub> and NO<sub>3</sub>

During the XIXIMI-6 campaign, the spatial distribution of macronutrients (PO<sub>4</sub> and NO<sub>3</sub>) was very close to that of Ni in the first 600 m (Figures 5A–C), with low concentrations in the surface layer (100 m) and then increased gradually with depth. An important difference between Ni and macronutrients in the surface waters was that NO<sub>3</sub> ( $0.056 \pm 0.050$   $\mu$ mol kg<sup>-1</sup>) and PO<sub>4</sub> ( $0.023 \pm 0.006$   $\mu$ mol kg<sup>-1</sup>) reached levels close to the detection limit ( $0.02$   $\mu$ mol kg<sup>-1</sup> for both nutrients), while the Ni concentration never fell below  $1.51$  nmol kg<sup>-1</sup>. Similarly to Ni, the lowest values of macronutrients were detected in surface waters of the LC and the anticyclonic LCEs region and, associated with TACW, there was an uprising of high nutrient concentration isolines from the Caribbean Sea to the Campeche Bay area. As a result, CSWr in Campeche Bay had

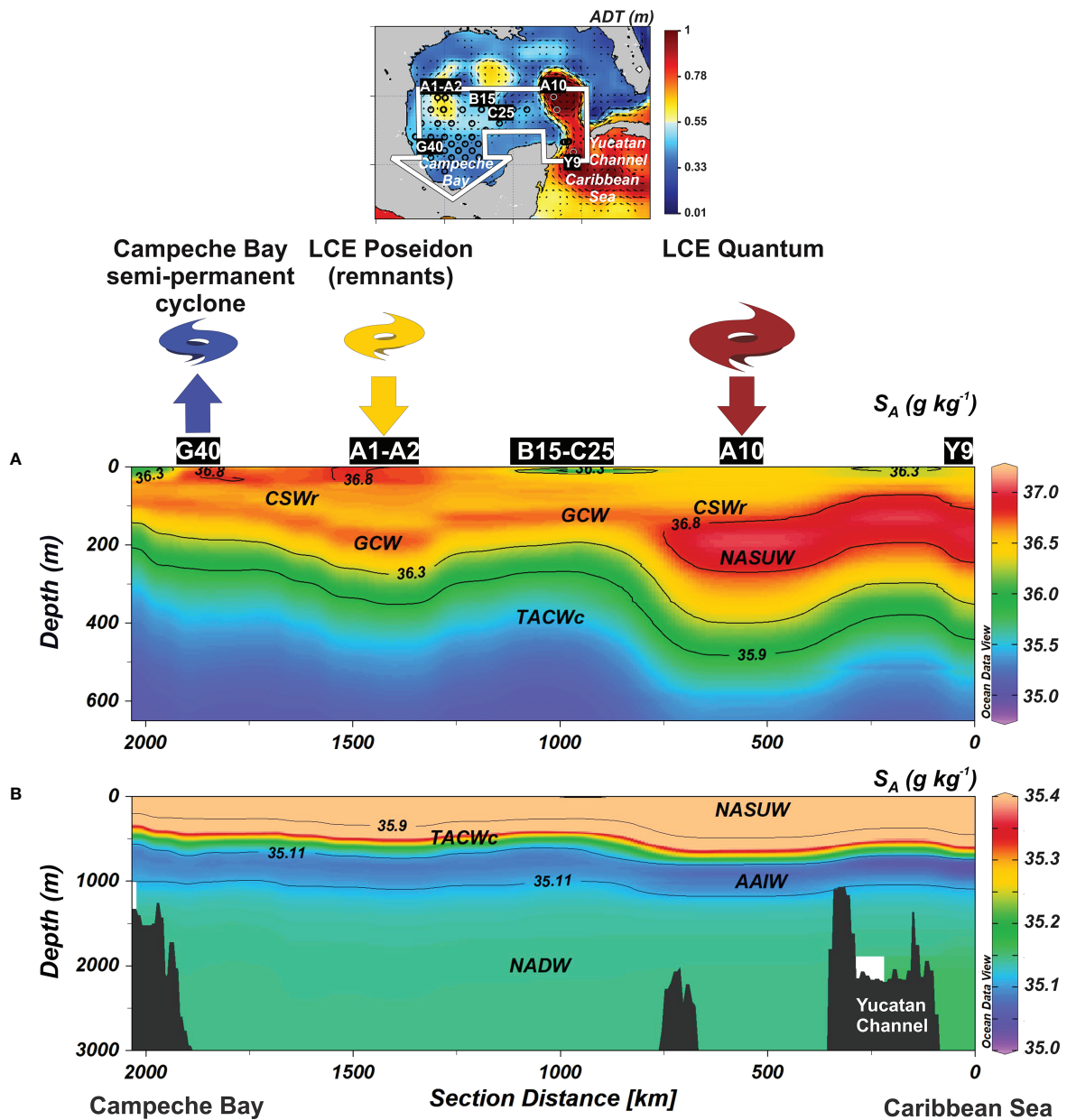


**FIGURE 3**  
 Sectional distribution of absolute salinity ( $S_A$ ) during the XIXIMI-6 cruise along a transect that begins in the Caribbean Sea and ends in the Gulf of Mexico in the Campeche Bay area: (A) from 0 to 600 m depth and (B) from 0 to 3500 m depth. The locations of the sampling stations marked in panel (A) are shown in the map above. The big white arrow shown on the map indicates the direction and extent of the transect. To improve the visual identification of water masses, the range of  $S_A$  values represented by the color scale is different for (A, B). The black solid contours indicate the isohaline boundaries of water masses based on the classification proposed by Portela et al. (2018). ADT, absolute dynamic topography; LCE, Loop Current eddy; CSWr, Caribbean Surface Water remnant; GCW, Gulf Common Water; NASUW, North Atlantic Subtropical Underwater; TACWc, Tropical Atlantic Central Water core; AAIW, Antarctic Intermediate Water; and NADW, North Atlantic Deep Water.

~13-fold more  $NO_3$  and ~2.5-fold more  $PO_4$  than in LC. Lastly, TACW was the water mass in the upper 600 m with highest potential to be the main source of  $PO_4$  ( $1.37 \pm 0.36\ \mu mol\ kg^{-1}$ ) and  $NO_3$  ( $22.4 \pm 4.8\ \mu mol\ kg^{-1}$ ) to the euphotic zone of the GoM (Figures 5B, C).

## 4 Discussion

The vertical distribution of Ni in the GoM was nutrient-like (Figure 4), which agrees well with what has been previously documented in the northeastern GoM (Boyle et al., 1984) and in

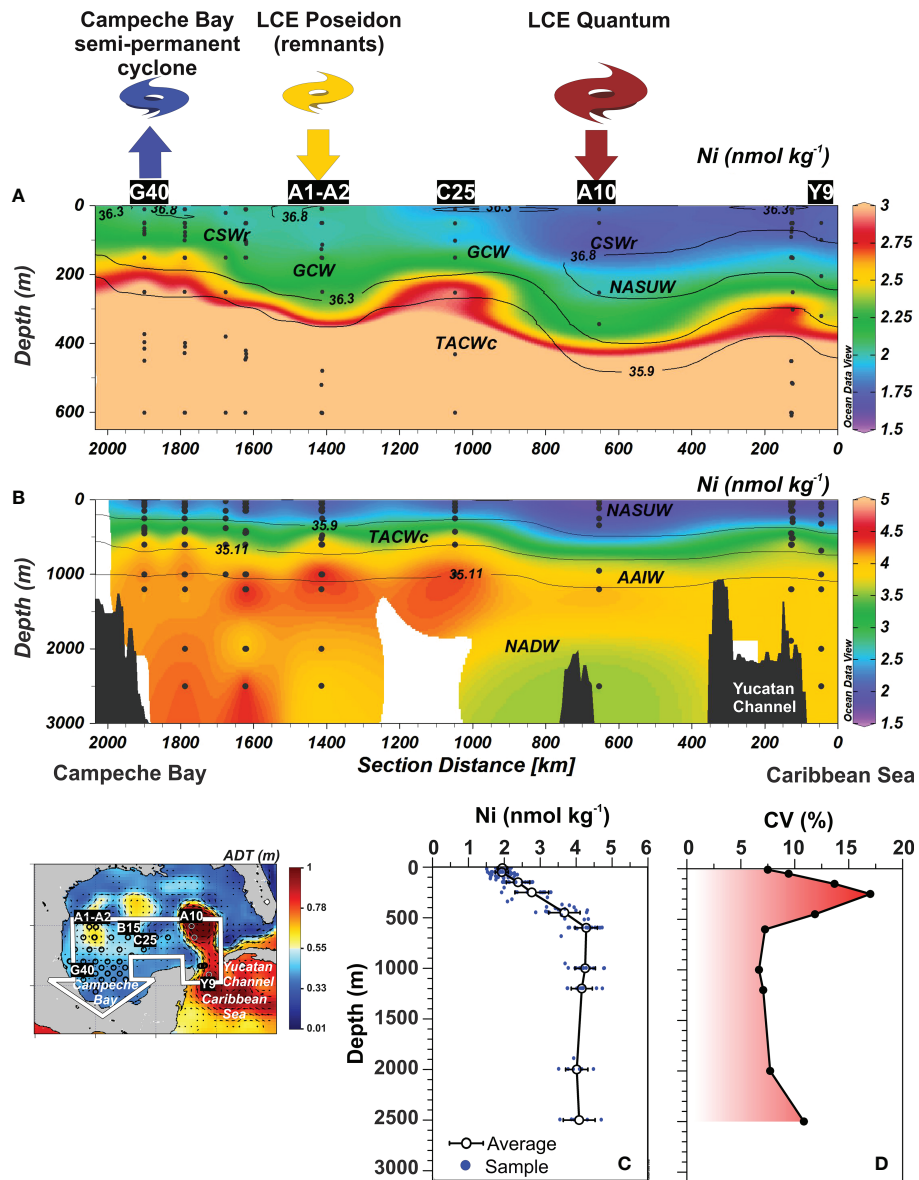


FIGURE 4

Sectional distribution of dissolved Ni along a transect that begins in the Caribbean Sea and ends in the Gulf of Mexico in the Campeche Bay area during the XIXIMI-6 cruise: (A) from 0 to 600 m depth and (B) from 0 to 3500 m depth. (C) Average vertical profile ( $\pm$  standard error) and (D) coefficient of variation (CV) of dissolved Ni for depths 10, 50, 150, 250, 450, 500, 1000, 1200, 2000, and 2500 m. The average profile was constructed using the dissolved Ni concentrations measured in the 22 stations sampled during the XIXIMI-6 cruise. The locations of the sampling stations marked in (A) are shown on the map. The big white arrow shown on the map indicates the direction and extent of the transect. To highlight the spatial differences in the Ni concentration in both shallow and deep waters, the range of Ni concentrations represented by the color scale is different for (A, B). The black solid contours in (A, B) indicate the isohaline boundaries of water masses based on the classification proposed by Portela et al. (2018). LCE, Loop Current eddy; ADT, absolute dynamic topography; CV, coefficient of variation; CSW<sub>r</sub>, Caribbean Surface Water remnant; GCW, Gulf Common Water; NASUW, North Atlantic Subtropical Underwater; TACW<sub>c</sub>, Tropical Atlantic Central Water core; AAIW, Antarctic Intermediate Water; and NADW, North Atlantic Deep Water.

the Atlantic Ocean (Yeats and Campbell, 1983; Bowie et al., 2002; Middag et al., 2020; Lemaitre et al., 2022). However, the high horizontal variability exhibited by the Ni profiles during the

XIXIMI-6 cruise distinguishes the deep-water region of the Gulf from other regions (Figures 4A-C). The horizontal variability of the Ni concentration was assessed by calculating the coefficient

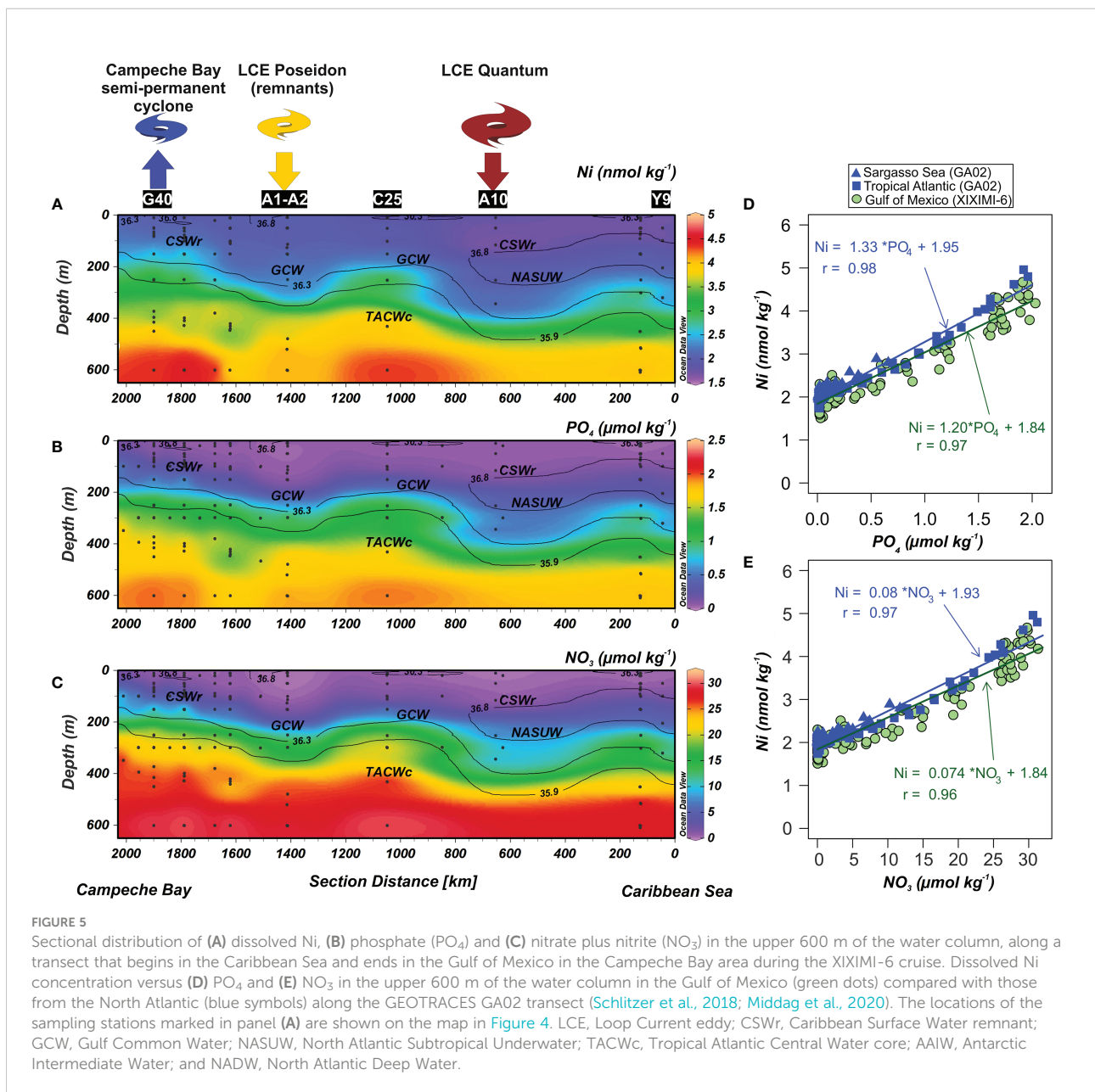
of variation (CV = standard deviation \* 100/average) for each depth horizon in the GoM. Figure 4D shows that the Ni levels in the first 600 m of the water column were significantly ( $p < 0.05$ ) more variable (CV < 17%) than those of deeper water (CV < 10%), which indicates that the greatest amount of horizontal variability was concentrated in the upper portion of the water column that is usually affected by mesoscale eddies (Meunier et al., 2018; Sosa-Gutiérrez et al., 2020; Valencia-Gasti et al., 2022). In the following sections, we will discuss: 1) the behavior of Ni in the GoM compared to that of the Atlantic Ocean; 2) the influence of mesoscale eddies on the vertical distribution of Ni in the Gulf; 3) the Ni relationship with macronutrients; and 4) the

impact of mesoscale eddies on the stock of Ni in the surface layer of the GoM and its biogeochemical implications.

### 4.1 Distribution of dissolved nickel: Gulf of Mexico vs northwestern Atlantic Ocean

#### 4.1.1 The 0 - 100 m depth layer

Notable differences in the average Ni concentrations were observed in the upper 100 m layer from the LC and Campeche Bay (Figure 4A; Table 1). On the one hand, the lowest average Ni



concentrations in the GoM ( $1.71 \pm 0.11 \text{ nmol kg}^{-1}$ ) were recorded in the LC region and were similar to those of the surface waters of the Caribbean Sea ( $1.65 \pm 0.29 \text{ nmol kg}^{-1}$ ; Pinedo-Gonzalez et al., 2015). In contrast, the average surface levels of Ni ( $2.04 \pm 0.11 \text{ nmol kg}^{-1}$ ) in Campeche Bay were the highest measured in this study and are similar to those detected in the Sargasso Sea ( $2.04 \pm 0.02 \text{ nmol kg}^{-1}$ ; Table 1), which is an area impacted by Saharan dust deposition (Jickells et al., 1998; Shelley et al., 2012) and mesoscale eddies (Shelley et al., 2012; Conway et al., 2018; Sedwick et al., 2020).

#### 4.1.1.1 The region of the LC and anticyclone Quantum

In the region influenced by the LC and LCE Quantum, CSWr presented a slight impoverishment of Ni (~ 16%) relative to the levels measured in the Sargasso Sea and the same water mass in Campeche Bay (Figure 4A; Table 1). In particular, the lowest Ni concentrations were detected even deeper than 100 m in the area of the anticyclone Quantum (station A10) and the small anticyclone located in the Caribbean waters (station Y9; Figure 4A). These low Ni values could be explained by the combined effect of biologically mediated processes and mesoscale dynamics. Firstly, the trapping of upper water masses inside anticyclonic eddies (e.g., McGillicuddy, 2016) is a condition allowing the autotrophic community inhabiting the euphotic zone to consume and eventually decrease the reserves of Ni and macronutrients (Figures 1B, 2A; Linacre et al., 2019). Secondly, anticyclonic eddies deepen Ni- and nutrient-impoverished waters while avoiding their replenishment from beneath (Figures 1C-E, 5A-C; Lee-Sánchez et al., 2022; Velásquez-Aristizábal et al., 2022). Thirdly, Ni consumption (slower than that for macronutrients; John et al., 2022) will occur until the concentrations of  $\text{NO}_3$  and  $\text{PO}_4$  become limiting, creating over the time marine deserts characterized by very low Chl-a and NPP, such as those detected during XIXIMI-6 campaign (Figures 2C, D). The region of the LC and the adjacent Caribbean Sea is an oceanographic province whose hydrographic characteristics of warm temperatures and very low nutrients concentrations are maintained and, as a consequence, oligotrophic conditions are prevalent here. Thus, we believe that the scenario we found during the XIXIMI-6, with low values of Ni and macronutrients (and possibly other elements with nutrient-like distributions), is more common and almost permanent in this area. However, this hypothesis requires more data and remains to be proven.

#### 4.1.1.2 The region of Campeche Bay: Potential Ni inputs

Despite being more productive than the LC area (Figure 2C, D), in the euphotic zone of Campeche Bay were recorded slightly higher Ni concentrations, possibly due to an apparent balance between Ni consumption and replenishment (Figure 4A). In particular, the CSWr in Campeche Bay showed a clear Ni enrichment ( $\Delta\text{Ni} = 0.33$

$\text{nmol kg}^{-1}$ ) when compared with Ni concentrations measured at stations located in the LC region (Figure 4A; Table 1). This Ni enrichment could be the result of a) atmospheric deposition (e.g., Herut et al., 2016), b) fluvial contributions (e.g., Boyle et al., 1984), c) benthic fluxes from the shelf (e.g., Lenstra et al., 2022), d) organic matter remineralization (e.g., Middag et al., 2020), and/or e) mesoscale dynamics (e.g., Conway et al., 2018; Sedwick et al., 2020). In the case of eolian deposition, the Sahara Desert is potentially the most important source of dust to the GoM (Lenes et al., 2012; Hayes et al., 2022). However, considering the Ni concentration of Saharan dust ( $0.46 \mu\text{mol g}^{-1}$ ; Herut et al., 2016) and its solubility in seawater (60%; Fishwick et al., 2018), a constant deposition rate ( $12.2 \text{ mg m}^{-2} \text{ d}^{-1}$ ; Lenes et al., 2012) during a period of three months (i.e., travel time for LCEs across the GoM; Oey et al., 2005) could increase the Ni concentration in the upper 100 m of the water column by only  $2.96 \text{ pmol kg}^{-1}$ . On the other hand, the impact of the fluvial contribution of Ni to the GoM can be distinguished by changes in salinity in surface waters, with low salinities usually being associated with high Ni concentrations (e.g., Boyle et al., 1984; Wen et al., 2011). Nevertheless, during the XIXIMI-6 campaign, no low-salinity features were detected (Figure 3A), which may indicate that the fluvial contributions of Ni was limited to the coastal zone. Likewise, the continental shelf sediments could be a source of metals to nearshore stations. For example, Lenstra et al. (2022) reported a benthic flux of Ni of  $1.7 \mu\text{mol m}^{-2} \text{ d}^{-1}$  for one nearshore station (16 m depth) on the continental shelf of Louisiana. This flux could increase the Ni concentration by  $1.5 \text{ nmol kg}^{-1}$  in the upper 100 m of the GoM during a period of 3 months and without Ni consumption. Clearly, this Ni addition would be higher compared with the Ni enrichment observed in Campeche Bay. However, during the XIXIMI-6 campaign, Ni concentrations in the upper 100 m were never  $> 2.4 \text{ nmol kg}^{-1}$  and there were no high values evidencing that Ni-rich plumes had been advected from the continental shelf in Campeche Bay (Figure 1C), probably because the shelf in this area is narrower than in the northern Gulf (Figure 1A). Thus, as it has been reported for other marginal seas (e.g., Middag et al., 2022; Seo et al., 2022) and productive nearshore waters (Liu et al., 2022), the shelf sediments appear to be a limited Ni source to the upper water column of the deep-water region of the GoM. Additionally, the remineralization of organic matter might contribute dissolved Ni to the water column as waters travel from the Caribbean into the interior of the Gulf. To explore this idea, we chose the upper section of TACW ( $\sigma_t = 26 - 26.5 \text{ kg m}^{-3}$ ) to perform an isopycnal analysis of the relationship between dissolved Ni (and  $\text{PO}_4$ ) and apparent oxygen utilization (AOU) in LC and Campeche Bay (see Supplementary Table S2). At first sight, higher values of AOU, Ni and  $\text{PO}_4$  recorded in Campeche Bay would suggest that remineralization might be taking place along the density anomaly layer during its transit from the LC area to Campeche Bay in the inner side of the Gulf. However, we found that this isopycnal layer was warmer ( $\Delta T = 1.54 \pm 0.17^\circ\text{C}$ ) and saltier ( $\Delta S_A = 0.302 \pm 0.099 \text{ g kg}^{-1}$ ) in the LC area, suggesting the presence of an important

fraction of water from the surface; whereas Campeche Bay had a higher proportion of water from below, which is colder and fresher. We took advantage of the fact that all these variables had a strong linear relationship with temperature ( $r^2 > 0.85$ ) to provide evidence of this vertical transport of water. Table S2 shows that the expected values of Ni (also for AOU and  $\text{PO}_4$ ) are very similar to those predicted using the temperature measured in the layer (Supplementary Table S2). These findings reveal that the differences in Ni and AOU between these two areas can be explained by mixing and the vertical displacement of the water masses and not by remineralization. This interpretation is consistent with a recent study indicating that Ni regeneration of organic matter from the GoM was slow and resulted in very low Ni increases after 6 months of incubation when compared to the baseline amount of this element (Hollister et al., 2020). Similarly, Middag et al. (2020) reported that the influence of remineralization on the Ni distribution in the Atlantic is relatively limited (13%) while the slow regeneration of Ni plays an important role in explaining the global distribution of this element (John et al., 2022).

In this context, one alternative explanation for the Ni enrichment of CSWr observed in Campeche Bay, is the eddy-Ekman pumping of Ni-rich subsurface waters to the euphotic zone promoted by the semi-permanent cyclonic eddy of this region (Pérez-Brunius et al., 2013; Linacre et al., 2015). Thus, considering the Ni concentration of the water mass underneath CSWr (GCW:  $2.16 \text{ nmol kg}^{-1}$ ; Table 1), we estimated that vertical velocities on the order of  $0.17 \text{ m d}^{-1}$  would increase the levels of Ni in the upper 100 m layer by  $0.33 \text{ nmol kg}^{-1}$  in a period of 3 months. This increase corresponds to the enrichment of Ni in the CSWr within Campeche Bay. Our calculation is reasonable given that it is within the range of values of eddy-induced Ekman pumping estimated for mesoscale eddies in the North Atlantic ( $0.1\text{--}1.0 \text{ m d}^{-1}$ ; Martin and Richards, 2001) and in other regions of the world (e.g.,  $\sim 0.1 \text{ m d}^{-1}$  in the South Indian Ocean; Gaube et al., 2013). This eddy-driven circulation associated with the wind stress curl is the mechanism that maintains the cyclonic circulation in the Campeche Bay (Vázquez de la Cerda et al., 2005). In terms of the vertical flux of Ni, the eddy-Ekman pumping generated by the semi-permanent cyclone of Campeche Bay would be responsible for a Ni flux of  $0.37 \mu\text{mol m}^{-2} \text{ d}^{-1}$  (110 times higher compared with the atmospheric flux of soluble Ni of  $3.37 \times 10^{-3} \mu\text{mol m}^{-2} \text{ d}^{-1}$ ), which supports the hypothesis that mesoscale dynamics may explain the spatial differences in Ni concentrations observed in the first 100 m of the GoM.

#### 4.1.2 Below the 100 m layer

In general, our Ni profiles in the 100 – 1000 m depth layer were similar to one of the few Ni deep profiles available in the literature for the GoM (Boyle et al., 1984; star symbols in Figure 6A). However, Ni profiles in the Caribbean (Y9) and LCE Quantum (A10) stations, showed lower concentrations

than those of the regions influenced by the remnants of the LCE Poseidon (A1, A2), Campeche Bay (G40, G42), and the Boyle et al's Ni profile. The wide range of horizontal variation shown by the distribution of Ni in the GoM (Figure 6A; Table 1) was delimited by the values of Ni profiles from the tropical Atlantic and the Sargasso Sea reported by GEOTRACES (GA02 cruise; Schlitzer et al., 2018; Middag et al., 2020), which demonstrates the notable presence of the Atlantic water masses within the GoM. Similarly, Ni profiles from the northwestern Atlantic Ocean (pink and gray lines in Figure 6A) also show a marked horizontal variability and, as in the GoM, the differences between the Sargasso Sea and the tropical Atlantic are accentuated within the 100 - 1000 m layer. The variability shown by Ni profiles in the tropical Atlantic could be related to the impact of mesoscale eddies released from the North Brazil Current (Fratantoni and Richardson, 2006). Additionally, between  $10^\circ \text{ N}$  and  $20^\circ \text{ N}$  there is a progressive deepening and erosion of the Ni-rich AAIW as latitude increases in the transect GA02 (Figures 6A, C; Middag et al., 2020), increasing the Ni variability in the western tropical Atlantic. In the case of the Sargasso Sea, mesoscale eddies have been found to modify the vertical distributions of water masses with different amounts of dissolved Fe and consequently control the availability of this element in the euphotic zone (e.g., Shelley et al., 2012; Conway et al., 2018; Sedwick et al., 2020). Likewise, eddy-driven dynamics associated with the intrusion of the LC into the GoM and the shedding of mesoscale LCEs, could explain the wide range of horizontal variation showed by Ni profiles in the deep-water region of the Gulf, as discussed in the following section. On the other hand, in marked contrast to what was observed in surface and intermediate waters, the deep waters of the GoM ( $> 1000 \text{ m}$ ) exhibited Ni concentrations that were less variable and with magnitudes similar to those reported by GEOTRACES (GA02 cruise; Schlitzer et al., 2018; Middag et al., 2020) for the deep waters of the tropical Atlantic and the Sargasso Sea (Figure 6A; Table 1).

## 4.2 Influence of mesoscale dynamics on the distribution of dissolved Ni in the Gulf of Mexico

The high variability shown by Ni profiles in the first 1000 m of the GoM could be closely related to the physical mesoscale dynamics that characterize the Gulf (Elliott, 1982; Biggs et al., 1996; Meunier et al., 2018) as has been reported for other physical (Valencia-Gasti et al., 2022), chemical (Hernández-Candelario et al., 2019; Lee-Sánchez et al., 2022; Velásquez-Aristizábal et al., 2022), and biological (e.g., Salas-de-León et al., 2004; Linacre et al., 2015; Durán-Campos et al., 2017) properties. Particularly, mesoscale eddies can sink or raise water masses depending on their spin direction: cyclonic eddies produce an upward flux of subsurface waters towards the euphotic zone,

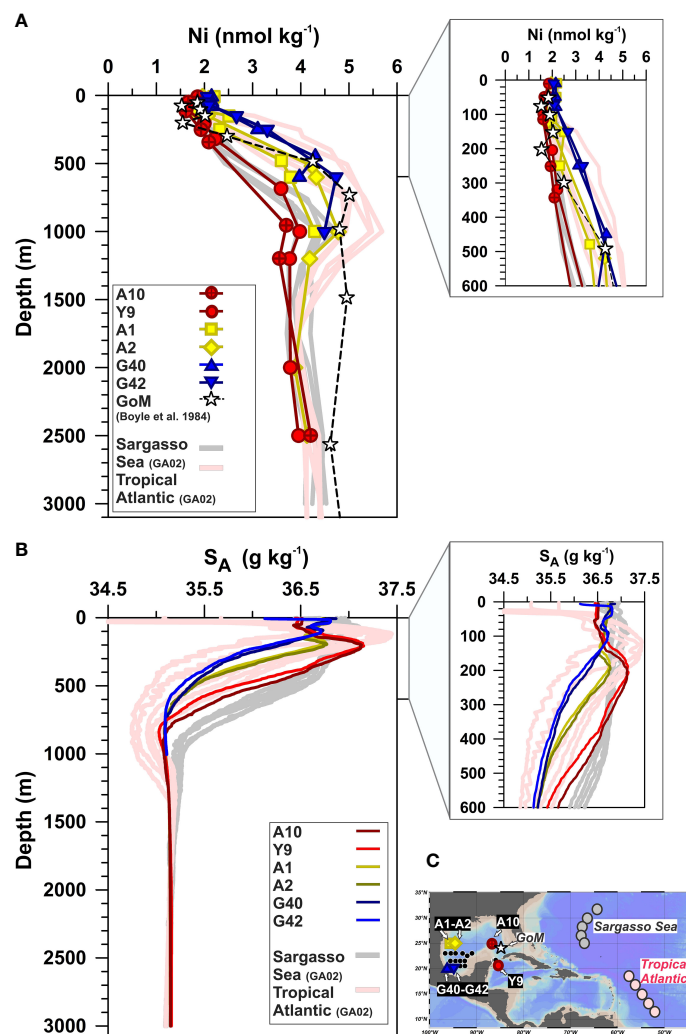


FIGURE 6

Vertical profiles of (A) dissolved Ni and (B) absolute salinity ( $S_A$ ) during the XIXIMI-6 cruise. For comparison, the vertical profiles of dissolved Ni reported for the eastern GoM (Boyle et al., 1984; star symbols), as well as the dissolved Ni and  $S_A$  in the North Atlantic (Sargasso Sea and Tropical North Atlantic) from the GEOTRACES GA02 transect (Schlitzer et al., 2018; Middag et al., 2020) are included in (A, B), respectively. The locations of the sampling stations are shown on the map (C). Note that profiles of dissolved Ni (A) and  $S_A$  (B) in the upper 600 m are enlarged to improve visualization.

while anticyclonic eddies do the opposite (McGillicuddy, 2016). The sectional distribution of Ni during XIXIMI-6 reveals that the locations of anticyclonic and cyclonic eddies are associated with the vertical displacement of water masses with different levels of this element in the first 600 m (Figure 4A), which provides a clue to explain the high variability shown by Ni profiles (Figure 6A).

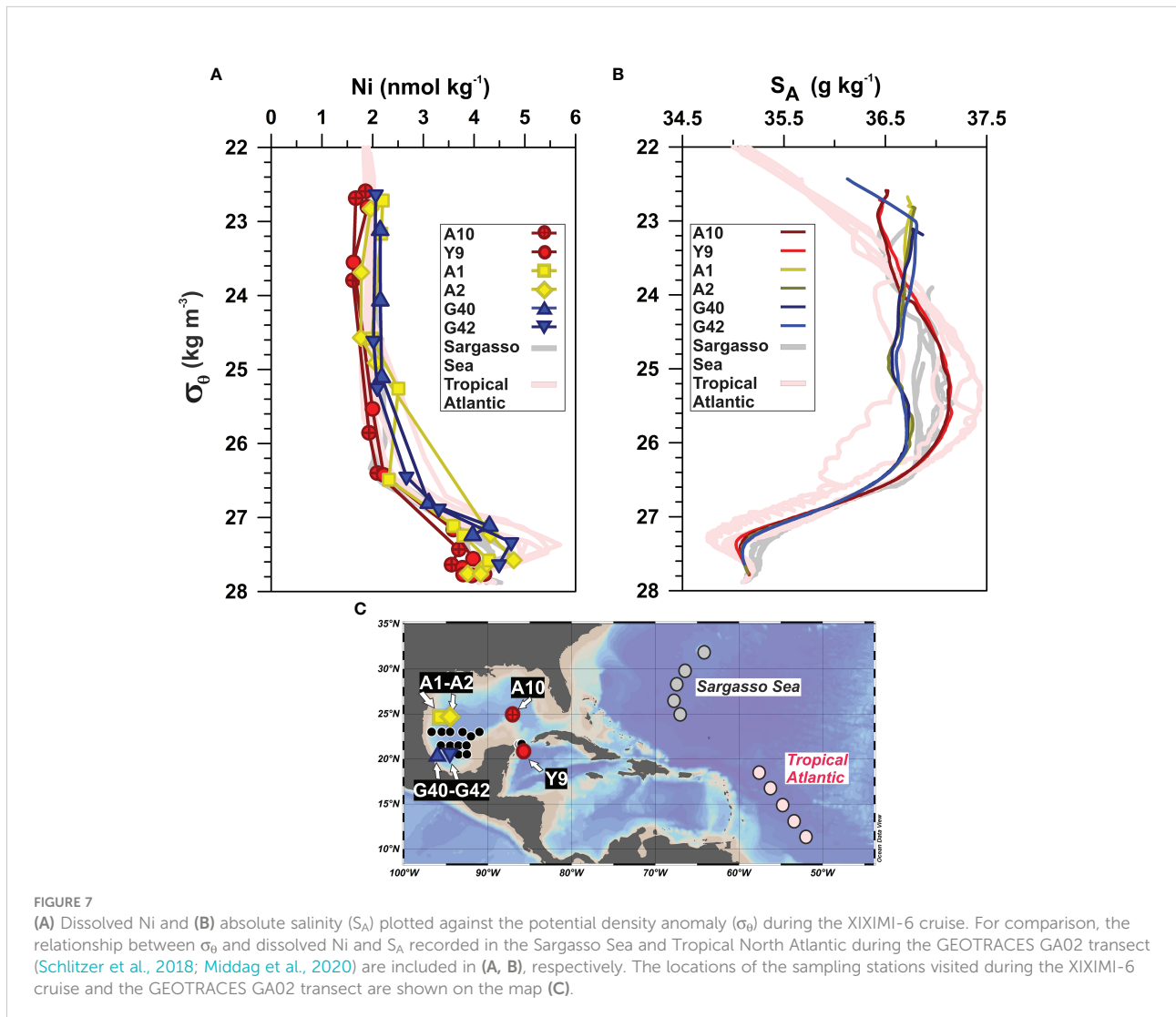
Except for the CSWr, the average Ni concentrations of the water masses in the first 600 m did not show significant differences ( $p > 0.05$ ) among the three regions identified during the cruise (Table 1). This means that mesoscale dynamics, rather than biogeochemical processes likely constitute an important factor controlling the high spatial variability of dissolved Ni in

the GoM. If this is the case, the vertical distributions of conservative variables, such as  $S_A$ , could help to explain this relationship with mesoscale dynamics. Figure 6B shows that the  $S_A$  profiles of the GoM were highly variable with marked differences between LC stations and those in the interior of the GoM. The range of variation in  $S_A$  profiles in the surface and intermediate waters of the Gulf was delimited by the values of the less salty waters of the tropical Atlantic and those of the Sargasso Sea, which had greater salinity (Figure 6B; Schlitzer et al., 2018; Middag et al., 2020). It is important to note that the  $S_A$  profiles in the northwestern Atlantic Ocean (pink and gray lines in Figure 6B) also showed high horizontal variability associated with the influence of the mesoscale eddies in that

region. In contrast, the deep waters (> 1000 m) of the GoM exhibited salinities that were very close to those reported for the deep waters of the Atlantic Ocean (Figure 6B; Schlitzer et al., 2018; Middag et al., 2020). Given that the vertical distribution of  $S_A$  exhibited horizontal variability that was very similar to that of the Ni profiles, mesoscale eddies appear to constitute the main controlling factor that determines the distribution of Ni in the GoM. Considering that mesoscale eddies have the ability to sink or raise isopycnals (McGillicuddy, 2016), one way to subtract the effect of mesoscale dynamics is to compare the  $S_A$  and Ni levels against the potential density anomaly (e.g., Hernández-Candelario et al., 2019). Figure 7 shows that the high spatial variability shown by Ni and  $S_A$  in the surface and intermediate waters of the GoM (Figure 6) decreases substantially when both variables are plotted against potential density anomalies. This can also be seen in terms of the coefficient of variation, with lesser variability of Ni along each potential density anomaly horizon (CV: 4–11%) compared to higher variability of Ni values

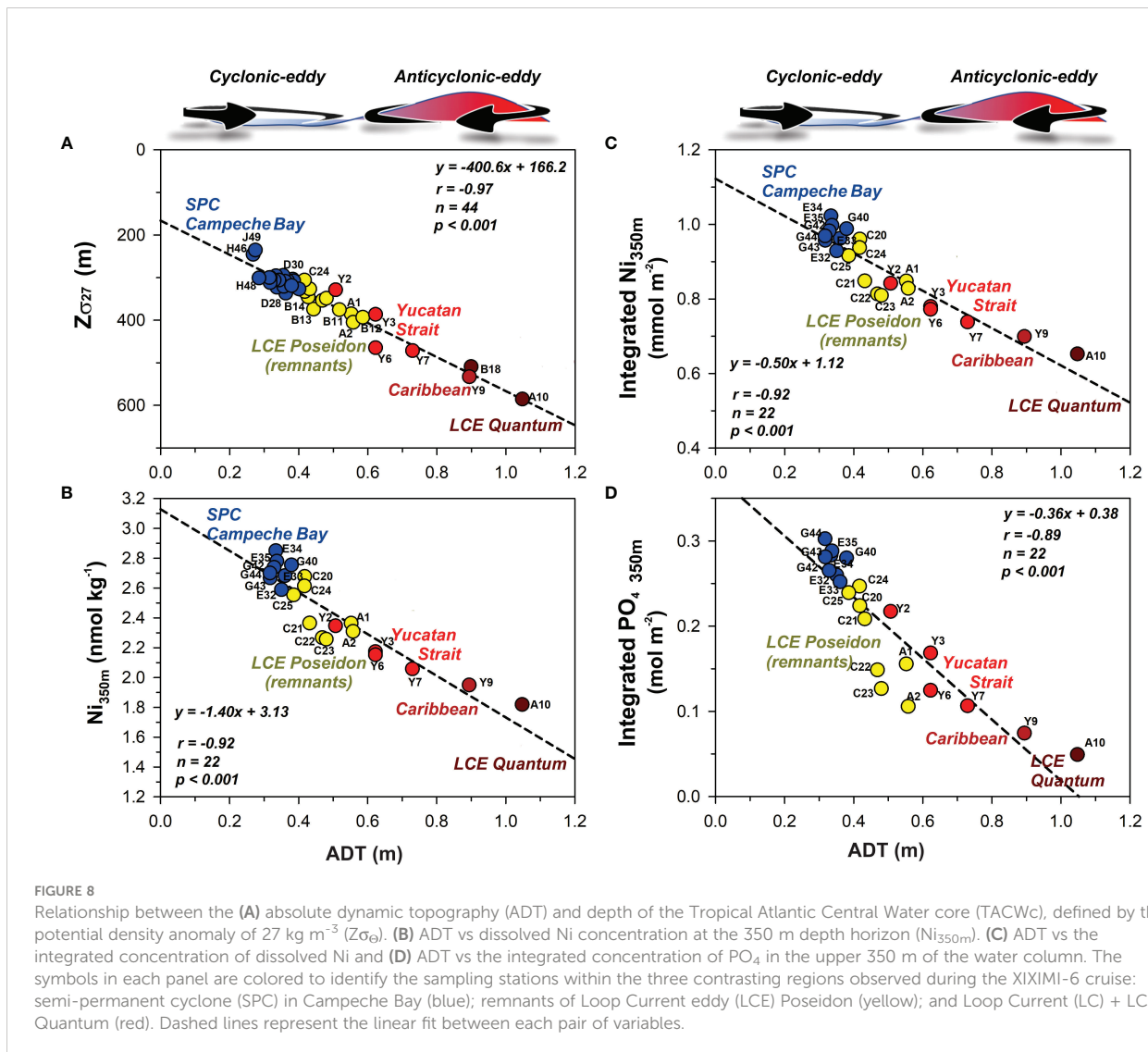
in each depth horizon (CV: 7–17%; Figure 4D), implying that mesoscale eddies play an important role in controlling the vertical distribution of Ni in the GoM.

Similarly, ADT can be used as an indicator of the type of mesoscale circulation that characterizes the surface waters of the GoM. High ADT values are associated with anticyclonic eddies or their remnants, whereas low ADT values are associated with cyclonic eddies (Oey et al., 2005; McGillicuddy, 2016; Figure 2A). To quantitatively assess the effects of mesoscale eddies on the Ni distribution in the GoM, a correlation analysis between ADT and the depth of the TACW core was conducted. The TACW core, identified by the potential density anomaly of  $27 \text{ kg m}^{-3}$  (Portela et al., 2018), was selected for this analysis because it meets the following criteria: 1) it was present in all three regions identified during the XIXIMI-6 campaign; 2) TACW has high Ni concentrations (Table 1) and its impact on surface waters will depend on its position (depth) within the water column; 3) it is located below the euphotic zone and therefore Ni removal by



primary producers can be neglected; 4) considering the low adsorption/scavenging of Ni by particles (Archer et al., 2020; Middag et al., 2020), mixing with other water masses with lower Ni concentrations is the only process potentially capable of decreasing the Ni concentration in TACW; and 5) this water mass is far removed from the influence of important sources of Ni located either at depth (e.g., benthic inputs) or at the surface (e.g., atmospheric deposition, fluvial inputs, and anthropogenic inputs; Morley et al., 1997; Herut et al., 2016). Our analysis indicates that the relationship between ADT and the depth of the TACW core during our study period was highly significant ( $p < 0.001$ ; Figure 8A). In the area of the LC and the anticyclonic LCE Quantum, elevated ADT values were associated with a deepening of the TACW core of  $\sim 400$  m relative to its position in Campeche Bay, where low ADT values were associated with the presence of the semi-permanent cyclonic eddy (Durán-Campos et al., 2017). In addition, correlation analyses were performed between the Ni

concentration at 350 m and ADT (Figure 8B) and between the concentration of Ni integrated in the first 350 m of the water column and ADT (Figure 8C). As can be seen in Figures 8B, C, elevated ADT values were associated with Ni-impoverished stations, and conversely low ADT values were linked to stations with higher Ni concentrations ( $r = -0.92$ ;  $p < 0.001$ ). Interestingly, the anticyclonic LCE Quantum was able to decrease the Ni stock by  $\sim 65\%$  compared to that observed in Campeche Bay (Figures 1C, 8C). These results are highly relevant given that they quantitatively demonstrate the influence of mesoscale eddies on the Ni inventory in the surface waters of the GoM and provide a starting point to predict both the depth of the TACW core and the concentration of Ni integrated in the first 350 m of the water column by means of ADT satellite images. In addition, it is worth noting that mesoscale eddies also affect the macronutrient inventories in the upper 350 m of the GoM (Figures 1D, E), in agreement with previous studies that have reported the impact of



eddies on the distribution of  $\text{NO}_3$  in offshore waters of the Gulf (Lee-Sánchez et al., 2022; Velásquez-Aristizábal et al., 2022). Thus, during the XIXIMI-6 cruise, elevated ADT values were associated with  $\text{PO}_4$ -depleted stations in the first 350 m (Figure 8D), and conversely low ADT values were linked to stations with higher  $\text{PO}_4$  concentrations ( $r = 0.89$ ;  $p < 0.001$ ).

### 4.3 The nickel: Macronutrient relationships

During the XIXIMI-6 cruise, the nutrient-type distribution of Ni was similar to those of macronutrients, showing significant correlations ( $p < 0.001$ ) with  $\text{PO}_4$  and  $\text{NO}_3$  in the first 600 m of the GoM (Figures 5D, E). This reflects that Ni is associated with the production of organic matter in the euphotic zone and its destruction at depth (Bruland, 1980; Bruland and Franks, 1983; Boyle et al., 1984). Comparatively, the Ni :  $\text{PO}_4$  ( $1.20 \pm 0.12 \text{ nmol } \mu\text{mol}^{-1}$ ) and Ni :  $\text{NO}_3$  ( $0.074 \pm 0.008 \text{ nmol } \mu\text{mol}^{-1}$ ) slopes in the GoM were very similar to the Ni :  $\text{PO}_4$  ( $1.33 \pm 0.19 \text{ nmol } \mu\text{mol}^{-1}$ ) and Ni :  $\text{NO}_3$  ( $0.080 \pm 0.012 \text{ nmol } \mu\text{mol}^{-1}$ ) slopes in the upper 600 m of the tropical Atlantic and the Sargasso Sea (Figures 5D, E; Schlitzer et al., 2018; Middag et al., 2020). All these figures are within the range of values reported in the literature. For instance, the Ni :  $\text{PO}_4$  slopes for the GA02 Atlantic meridional section varied from  $0.6 \text{ nmol } \mu\text{mol}^{-1}$  in the northern subpolar gyre to  $2.7 \text{ nmol } \mu\text{mol}^{-1}$  in Antarctic origin waters (Middag et al., 2020), whereas Ni :  $\text{PO}_4$  data from marginal seas (e.g., Japan Sea; Seo et al., 2022) and productive upwelling margins (Benguela Current), range from  $0.5$  to  $2.3 \text{ nmol } \mu\text{mol}^{-1}$  (Liu et al., 2022). An equivalent variation has been reported for the Ni :  $\text{NO}_3$  slope (from  $0.03 \text{ nmol } \mu\text{mol}^{-1}$  to  $0.10 \text{ nmol } \mu\text{mol}^{-1}$ ) in the Atlantic Ocean (Lemaitre et al., 2022). In general, changes in Ni:macronutrient stoichiometries in the water column reflect external inputs (e.g., shelf fluxes, atmospheric deposition), preferential consumption by primary producers, seasonal change of productivity conditions, preferential remineralization and the mixing of water masses (Cloete et al., 2019; Middag et al., 2020; Seo et al., 2022; Lemaitre et al., 2022; Liu et al., 2022). In the case of the GoM, the Ni:macronutrient slopes showed no indication of external Ni inputs (Figures 5D, E). The gentler slopes in the GoM relative to the Atlantic could be interpreted as an inefficient biological uptake of Ni relative to  $\text{PO}_4$  and  $\text{NO}_3$  (Seo et al., 2022). However, given that both regression lines increase their difference to deeper water and not at the surface (Figures 5D, E), these small deviations can be better explained by the advection and mixing of water masses to the GoM and/or a slower regeneration rate of Ni compared to that of macronutrients in deeper waters (John et al., 2022). For example, the Ni :  $S_A$  slopes showed a decreasing trend from the tropical Atlantic to the Sargasso Sea and the GoM, whereas the  $\text{PO}_4$  :  $S_A$  slopes did not (Supplementary Figure S1), indicating that as AAIW becomes saltier owing to its mixing with TACW, a decrease of the Ni:macronutrient slopes takes place (Figures 5D, E). This south to north decrease in the Ni :  $\text{PO}_4$  (and Ni :  $\text{NO}_3$ ) slopes in the Atlantic can be explained by the progressive

latitudinal decline of AAIW (Ni- and macronutrients-enriched) and the greater presence of central and northern subpolar waters with lower concentrations of these elements (Middag et al., 2020; Liu et al., 2022; Lemaitre et al., 2022). Furthermore, an analysis on the content of macronutrients and Ni in the TACW core shows that, in the GoM, this water mass has significantly more phosphate ( $\Delta\text{PO}_4 = 0.18 \mu\text{mol kg}^{-1}$ ) and nitrate ( $\Delta\text{NO}_3 = 2.3 \mu\text{mol kg}^{-1}$ ) than the core of the same water mass in the Sargasso Sea and the tropical Atlantic (Supplementary Figure S2). In contrast, Ni concentrations were not statistically different among these three areas and, consequently, lower Ni :  $\text{PO}_4$  ratios were recorded in the Gulf. These findings suggest that, although it seems that remineralization of organic matter is taking place ( $\Delta\text{NO}_3/\Delta\text{PO}_4 = 12.8$ ) along the pathway of TACW towards the GoM, the corresponding increase in Ni was not observed in our study. One possible reason is that the process of regeneration of Ni from the organic debris is very slow as has been previously demonstrated in incubation experiments (Hollister et al., 2020) or inferred from field studies (Middag et al., 2020; John et al., 2022). Even so, further studies are required to distinguish quantitatively the relative importance of the physical and biogeochemical processes to explain the difference in the Ni:macronutrient slopes between the Atlantic Ocean and the GoM.

### 4.4 Biogeochemical implications

Anticyclonic eddies detached from the LC in the GoM, often push oligotrophic Caribbean waters to depths that are light-limited, whereas cyclonic eddies fertilize surface waters and consequently increase phytoplankton biomass in the interior of the Gulf (Salas-de-León et al., 2004; Linacre et al., 2015; Durán-Campos et al., 2017; Brokaw et al., 2020; Lee-Sánchez et al., 2022). In this study, we found that mesoscale eddies affected the integrated concentration of Ni and macronutrients within the first 350 m of the GoM, whereas the integrated Ni:macronutrient relationships were not modified (Supplementary Figure S3). In particular, waters under the influence of LCEs showed a significant decrease of the Ni and macronutrient inventories compared to those of Campeche Bay (Figures 1C-E, 8C, D). Thus, primary producers living in waters under the influence of LCEs could be expected to be affected by this Ni and macronutrient decline. Therefore, a question arises as to whether an association between ADT (Figure 2A) and Chl-a (Figure 2C) during the XIXIMI-6 campaign might be observed using satellite images.

Figure 9A shows a negative and statistically significant correlation ( $p < 0.001$ ) between ADT and Chl-a, which suggests a possible association between both variables. One explanation for this association is that the eddy-influenced availability of Ni and macronutrients in the surface waters of the GoM is an important factor that in part controls the biomass of primary producers during summer. However, considering the constant biogeochemical evolution of the LCEs, this interpretation depends on what moment the cruise was carried out. The reduced surface

inventory of Ni and macronutrients within LCEs during the cruise, might be the consequence of a previous event of consumption of these elements by phytoplankton and their limited replenishment from beneath (Figures 1C-E). The high temperatures and the stratification of the surface-layer during summer maintain a nitrate-limited environment (N:P ratios < 5), condition necessary for the proliferation of primary producers that require alternative sources of nitrogen (urea or N<sub>2</sub>) to grow (Linacre et al., 2019; Hernández-Sánchez et al., 2022). Thus, considering the fundamental role that Ni plays in the transformation of urea to ammonium (Price and Morel, 1991; Egleston and Morel, 2008; Dupont et al., 2010; Twining et al., 2012) and N<sub>2</sub> fixation (Ho, 2013; Lemaitre et al., 2022), a high demand of Ni could explain the low Ni inventories found in the first 350 m of the water column in the LCEs area (Figures 1C, 8C). This Ni drawdown possibly affect the development of phytoplankton blooms as suggested by the statistically significant correlation found between Chl-a and integrated Ni during the cruise (Figure 9B). It should be kept in mind that even though Ni concentrations never fell below 1.51 nmol kg<sup>-1</sup> within the GoM, it has been proposed that much of the dissolved Ni inventory that appears to be non-limiting at the surface is actually inaccessible to marine microbes (Mackey et al., 2002; Dupont et al., 2010; Morel et al., 2014; Archer et al., 2020; Middag et al., 2020). This intriguing Ni left over has been partially explained by the formation of Ni complexes with organic ligands, which are apparently unavailable to phytoplankton (Wen et al., 2006; Dupont et al., 2010; Boiteau et al., 2016; Archer et al., 2020) and, recently, by a slower biological uptake of Ni compared to that of macronutrients (John et al., 2022). Although our experimental design did not consider studying specifically this fraction of Ni, an indication of low Ni availability for marine organisms during the campaign in the Gulf could be the high integrated Ni : PO<sub>4</sub> ratios (>4 nmol mol<sup>-1</sup>; Figure 9C; Mackey et al., 2002) recorded in the LCEs region, an environment where nitrogen-limited conditions (Figures 1E, 5C) and very low Chl-a prevailed. Besides, it has recently been proposed that co-limitation by Ni and nitrogen might be present in large oceanic regions at low latitudes (Lemaitre et al., 2022), which may be the case in the surface waters of the GoM that are influenced by the LC and its anticyclonic eddies. Thus, once anticyclonic eddies are detached from the LC, transport Ni- and macronutrient-impoverished waters generating a significant effect on primary productivity, nitrogen fixation, and carbon cycling during their travel to the west in the Gulf. However, more research is needed to disentangle the complex interactions among Ni, the macronutrients and the biological activity in the GoM.

## 5 Conclusions

The XIXIMI-6 campaign was conducted in the deep-water region of the GoM during summer, in an oceanographic context that allowed to characterize three distinct regions in terms of physical dynamics (ADT and geostrophic velocity) and

biological conditions (Chl-a and NPP). The region encompassing the eastern portion of the GoM had the highest physical dynamics due to the strong influence of the LC and the anticyclonic LCE Quantum. The surface waters located in the core of the anticyclonic LCE Quantum were characterized by being the warmest while exhibiting the lowest Chl-a concentrations in the Gulf. On the other hand, the northwestern GoM was characterized by moderate physical dynamics that were related to the remnants of the anticyclonic LCE Poseidon and showed an incipient recovery of Chl-a and NPP levels. Finally, Campeche Bay was characterized by relatively weaker physical dynamics coupled with relatively higher biomass and primary productivity. The mesoscale eddies exerted a strong influence over the vertical distribution of the water masses in the first 1000 m of the water column. The first 600 m were dominated by warm Caribbean waters (CSWr), salty subtropical waters (NASUW), native Gulf waters (GCW), and tropical Atlantic waters (TACW). The vertical distributions of these water masses varied among the three regions of the GoM with a tendency to become shallower from the Yucatan Channel to Campeche Bay. This vertical rise was less evident with deeper water masses (> 1000 m).

In this context, the vertical distribution of Ni during the campaign was oceanographically consistent with a nutrient-like distribution in the global ocean, with low but never depleted values at the surface that gradually increased with depth until they reach a maximum between 600 and 1000 m depth. However, in the upper 600 m water column, Ni profiles showed high spatial variability, which was interpreted as a signal of the influence of mesoscale eddies. In the northeastern GoM, the anticyclonic LCE Quantum deepened Ni-poor Caribbean waters down to depths beyond the euphotic zone. In contrast, the semi-permanent cyclonic eddy of Campeche Bay raised isopycnals associated with deeper water masses (e.g., TACWc), pumping subsurface Ni-rich waters towards the euphotic zone. The low Ni concentrations in the LC and LCE eddies region were explained by the trapping of surface waters within anticyclonic eddies, the biological consumption of bioessential elements and their low replenishment from below due to the anticyclonic circulation. However, even under the influence of LCEs, surface Ni concentrations never fell below 1.51 nmol kg<sup>-1</sup>, which suggest the low lability of this element or alternatively, that its biological consumption becomes limited by the availability of the quickly consumed macronutrients. On the contrary, in Campeche Bay, the biological consumption of Ni was apparently overwhelmed by their replenishment promoted by the semi-permanent cyclonic circulation present there. Likewise, the spatial distribution of macronutrients (PO<sub>4</sub> and NO<sub>3</sub>) was very close to that of Ni, with Ni:macronutrient stoichiometries parallel to those reported for the Sargasso Sea and the tropical Atlantic. Mesoscale eddies similarly affected the Ni and macronutrient concentrations but without modifying their stoichiometries. In addition, the eddy-induced vertical

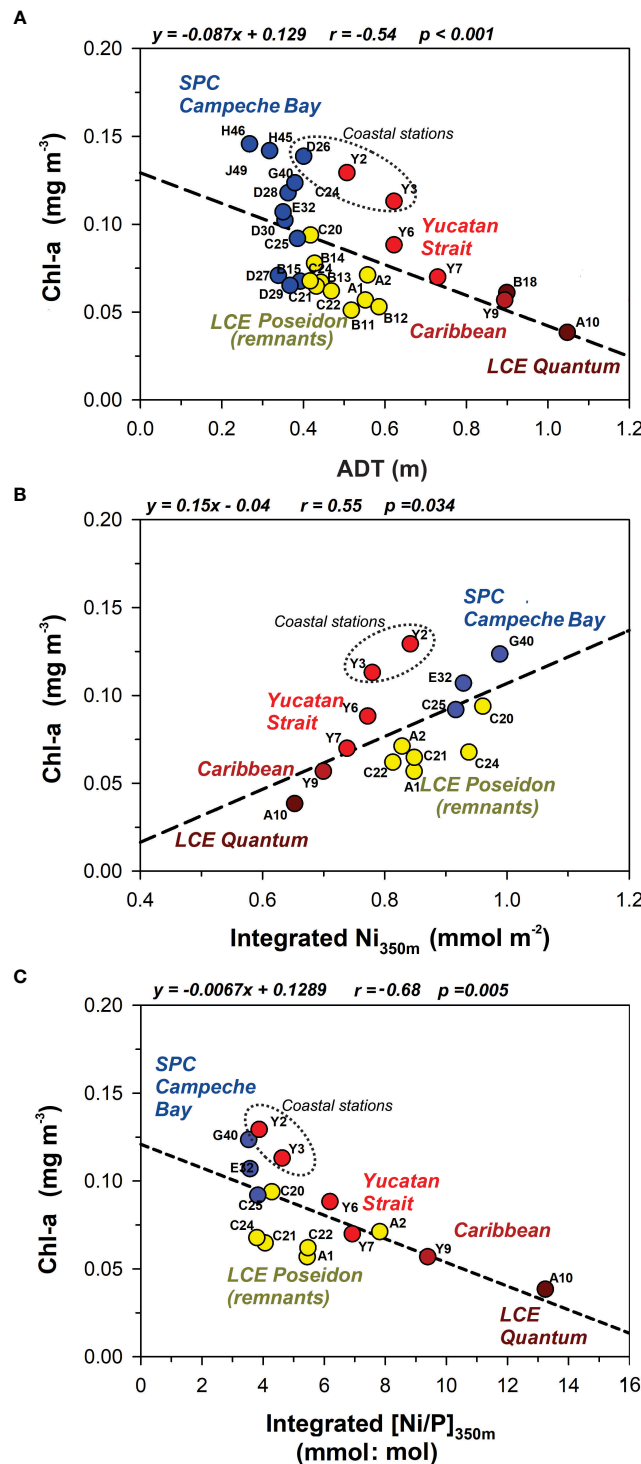


FIGURE 9

Relationship between satellite-derived chlorophyll a (Chl-a) and the variables of (A) absolute dynamic topography (ADT), (B) the integrated concentration of dissolved Ni in the first 350 m of the water column and (C) the ratio of the integrated Ni and PO<sub>4</sub> concentrations for the upper 350 m of the water column ( $\text{Ni}/\text{P}$ ). The Chl-a values were extracted from the 21-days composite image obtained for the XIXIMI-6 cruise (Figure 2C). The number of stations in panel (B) and (C) is < 22 due to limitations in the availability of satellite-derived Chl-a data (Figure 2C). The symbols in each panel are colored to identify the sampling stations within the three contrasting regions observed during the XIXIMI-6 cruise: semi-permanent cyclone (SPC) in Campeche Bay (blue); remnants of Loop Current eddy (LCE) Poseidon (yellow); and Loop Current (LC) + LCE Quantum (red). Dashed lines represent the linear fit between each pair of variables.

displacement of water masses resulted in a significant decrease of the Ni and macronutrients inventories in surface waters influenced by the LCE Quantum when compared to those of Campeche Bay. A decrease of such magnitude is very likely to affect the primary producers thriving in the northeastern portion of the GoM. In fact, a significant positive correlation between the integrated Ni concentration and satellite Chl-a suggests that Ni availability (along with other elements such as nitrogen and phosphorous) could have an effect on primary producers that inhabit the warm and oligotrophic waters of the GoM during summer. Future work to better assess the effect of Ni availability on primary producers in the GoM could help to unravel the complex interactions between this element, the macronutrients and biological activity in the marine environment.

## Data availability statement

The raw data (hydrography and dissolved Ni) supporting the conclusions of this article are included in the article/[Supplementary Material \(Table S1\)](#). Further inquiries can be directed to the corresponding author or to the Gulf of Mexico Research Consortium (CIGoM), which owns the data.

## Author contributions

FD-H, ML, MH-D, and VC-I designed the research and acquired the funding. ET-D organized the cruise and participated in the sampling. AF-B and ET-D performed the pre-concentration and AT-S carried out the Ni analysis by ICP-MS. VC-I performed the macronutrient analysis. AF-B, FD-H, ML, ET-D and VC-I performed the data curation. AF-B and FD-H processed and interpreted the data and wrote the manuscript with contributions provided by ML, MH-D, ET-D, AT-S, and VC-I. All authors contributed to the article and approved the submitted version.

## Funding

This research was funded by the Mexican National Council for Science and Technology-Mexican Ministry of Energy - Hydrocarbon Fund [project number 201441]. This is a contribution of the Gulf of Mexico Research Consortium

## References

Archer, C., Vance, D., Milne, A., and Lohan, M. C. (2020). The oceanic biogeochemistry of nickel and its isotopes: New data from the south Atlantic and the southern ocean biogeochemical divide. *earth planet. Sci. Lett.* 535, 116118. doi: 10.1016/j.epsl.2020.116118

(CIGoM). We acknowledge PEMEX's specific request to the Hydrocarbon Fund to address the environmental effects of oil spills in the Gulf of Mexico. Postdoctoral fellowships of AF-B were provided by the Mexican National Council for Science and Technology and CIGoM.

## Acknowledgments

We would like to thank the crew, the chief scientist Dr. S.Z. Herzka and the scientific party of the R/V Justo Sierra, for their work and support during the XIXIMI-6 cruise. We express our gratitude to M. Reyes and A. Gutierrez for their assistance during sampling at sea, to A. Gutierrez for its participation in the pre-concentration of Ni and to D. Sánchez-Quiles for its assistance in the dissolved Ni analysis by ICP-MS at the ICMAN-CSIC facilities. M.C. Aivila-Loópez and M. Muñoz-Anderson are also thanked for the macronutrient analysis. Finally, we are grateful to three reviewers for their insightful comments that significantly improved this manuscript.

## Conflict of interest

The authors declare that the research was conducted in the absence of any commercial or financial relationships that could be construed as a potential conflict of interest.

## Publisher's note

All claims expressed in this article are solely those of the authors and do not necessarily represent those of their affiliated organizations, or those of the publisher, the editors and the reviewers. Any product that may be evaluated in this article, or claim that may be made by its manufacturer, is not guaranteed or endorsed by the publisher.

## Supplementary material

The Supplementary Material for this article can be found online at: <https://www.frontiersin.org/articles/10.3389/fmars.2022.1036331/full#supplementary-material>

Armstrong, F. A. J., Stearns, C. R., and Strickland, J. D. H. (1967). The measurement of upwelling and subsequent biological processes by means of the technicon autoanalyzer and associated equipment. *Deep-Sea Res.* 14, 381–389. doi: 10.1016/0011-7471(67)90082-4

- Athié, G., Candela, J., Ochoa, J., and Sheinbaum, J. (2012). Impact of Caribbean cyclones on the detachment of loop current anticyclones. *J. Geophys. Res. Oceans*. 117, C3. doi: 10.1029/2011jc007090
- Badan, A. Jr., Candela, J., Sheinbaum, J., and Ochoa, J. (2005). "Upper-layer circulation in the approaches to Yucatan channel," in *Circulation in the gulf of Mexico: Observations and models*. Eds. W. Sturges and A. Lugo-Fernandez (Washington, DC: AGU, Geophys. Monogr. Ser.), 57–69.
- Biggs, D. C. (1992). Nutrients, plankton, and productivity in a warm-core ring in the western gulf of Mexico. *J. Geophys. Res. Oceans*. 97 (C2), 2143–2154. doi: 10.1029/90JC02020
- Biggs, D. C., Fargion, G. S., Hamilton, P., and Leben, R. R. (1996). Cleavage of a gulf of Mexico loop current eddy by a deep water cyclone. *J. Geophys. Res. Oceans*. 101 (C9), 20629–20641. doi: 10.1029/96JC01078
- Boiteau, R. M., Till, C. P., Ruacho, A., Bundy, R. M., Hawco, N. J., McKenna, A. M., et al. (2016). Structural characterization of natural nickel and copper binding ligands along the US GEOTRACES Eastern Pacific zonal transect. *Front. Mar. Sci.* 3. doi: 10.3389/fmars.2016.00243
- Bowie, A. R., Whitworth, D. J., Achterberg, E. P., Mantoura, R. F. C., and Worsfold, P. J. (2002). Biogeochemistry of Fe and other trace elements (Al, Co, Ni) in the upper Atlantic ocean. *Deep Sea Res. Part I. Oceanogr. Res. Pap.* 49 (4), 605–636. doi: 10.1016/S0967-0637(01)00061-9
- Boyle, E. A., Huested, S. S., and Jones, S. P. (1981). On the distribution of copper, nickel, and cadmium in the surface waters of the north-Atlantic and north Pacific-ocean. *J. Geophys. Res. Oceans*. 86 (C9), 8048–8066. doi: 10.1029/JC086iC09p08048
- Boyle, E. A., Reid, D. F., Huested, S. S., and Hering, J. (1984). Trace metals and radium in the gulf of Mexico: An evaluation of river and continental shelf sources. *Earth Planet. Sci. Lett.* 69, 69–87. doi: 10.1016/0012-821X(84)90075-X
- Brokaw, R. J., Subrahmanyam, B., Trott, C. B., and Chaigneau, A. (2020). Eddy Surface Characteristics and Vertical Structure in the Gulf of Mexico from Satellite Observations and Model Simulations. *J. Geophys. Res. Oceans*. 125 (2), e2019JC015538. doi: 10.1029/2019JC015538
- Brunland, K. W. (1980). Oceanographic distributions of cadmium, zinc, nickel, and copper in the north Pacific. *Earth Planet. Sci. Lett.* 47 (2), 176–198. doi: 10.1016/0012-821X(80)90035-7
- Brunland, K. W., and Franks, R. P. (1983). "Mn, Ni, Cu, Zn and Cd in the western north Atlantic," in *Trace metals in sea water*. Eds. C. S. Wong, E. Boyle, K. W. Brunland, J. D. Burton and E. D. Goldberg (Boston, MA: Springer), 395–414.
- Brunland, K. W., Franks, R. P., Knauer, G. A., and Martin, J. H. (1979). Sampling and analytical methods for the determination of copper, cadmium, zinc, and nickel at the nanogram per liter level in sea water. *Anal. Chim. Acta*. 105, 233–245. doi: 10.1016/S0003-2670(01)83754-5
- Candela, J., Ochoa, J., Sheinbaum, J., López, M., Pérez-Brunius, P., Tenreiro, M., et al. (2019). The flow through the gulf of Mexico. *J. Phys. Oceanogr.* 49 (6), 1381–1401. doi: 10.1175/jpo-d-18-01819.1
- Cloete, R., Loock, J. C., Mtshali, T., Fietz, S., and Roychoudhury, A. N. (2019). Winter and summer distributions of copper, zinc and nickel along the international GEOTRACES section GIPY05: Insights into deep winter mixing. *Chem. Geol.* 511, 342–357. doi: 10.1016/j.chemgeo.2018.10.023
- Conway, T. M., Palter, J. B., and de Souza, G. F. (2018). Gulf stream rings as a source of iron to the north Atlantic subtropical gyre. *Nat. Geosci.* 11, 594–598. doi: 10.1038/s41561-018-0162-0
- Cutter, G., Casciotti, K., Croot, P., Geibert, W., Heimbürger, L. E., Lohan, M., et al. (2017). *Sampling and sample-handling protocols for GEOTRACES cruises. version 3* (Toulouse: GEOTRACES International Project Office). doi: 10.25607/OBP-2
- Danielsson, L. G., Magnusson, B., and Westerlund, S. (1985). Cadmium, copper, iron, nickel and zinc in the north-east Atlantic ocean. *Mar. Chem.* 17, 23–41. doi: 10.1016/0304-4203(85)90034-9
- Delgadillo-Hinojosa, F., Camacho-Ibar, V., Huerta-Díaz, M. A., Torres-Delgado, V., Pérez-Brunius, P., Lares, L., et al. (2015). Seasonal behavior of dissolved cadmium and Cd/PO<sub>4</sub> ratio in todos santos bay: A retention site of upwelled waters in the Baja California peninsula, Mexico. *Mar. Chem.* 168, 37–48. doi: 10.1016/j.marchem.2014.10.010
- Delgadillo-Hinojosa, F., Segovia-Zavala, J. A., Huerta-Díaz, M. A., and Atilano-Silva, H. (2006). Influence of geochemical and physical processes on the vertical distribution of manganese in gulf of California waters. *Deep Sea Res. Part I. Oceanogr. Res. Pap.* 53 (8), 1301–1319. doi: 10.1016/j.dsr.2006.06.002
- Dominguez-Rosas, A. (2008). "Distribución vertical y temporal del níquel y cadmio en el golfo de California," in *Master's thesis in coastal oceanography* (Ensenada (BC: Universidad Autónoma de Baja California).
- Dupont, C. L., Buck, K. N., Palenik, B., and Barbeau, K. (2010). Nickel utilization in phytoplankton assemblages from contrasting oceanic regimes. *Deep Sea Res. Part I. Oceanogr. Res. Pap.* 57 (4), 553–566. doi: 10.1016/j.dsr.2009.12.014
- Durán-Campos, E., Salas-de-León, D. A., Monreal-Gómez, M. A., and Coria-Monter, E. (2017). Patterns of chlorophyll-a distribution linked to mesoscale structures in two contrasting areas Campeche canyon and bank, southern gulf of Mexico. *J. Sea Res.* 123, 30–38. doi: 10.1016/j.seares.2017.03.013
- Egleston, E. S., and Morel, F. M. (2008). Nickel limitation and zinc toxicity in a urea-grown diatom. *Limnol. Oceanogr.* 53 (6), 2462–2471. doi: 10.4319/lo.2008.53.6.2462
- Elliott, B. A. (1982). Anticyclonic rings in the gulf of Mexico. *J. Phys. Oceanogr.* 12 (11), 1292–1309. doi: 10.1175/1520-0485(1982)012<1292:ARITGO>2.0.CO;2
- Félix-Bermúdez, A., Delgadillo-Hinojosa, F., Torres-Delgado, E. V., and Muñoz-Barbosa, A. (2020). Does sea surface temperature affect solubility of iron in mineral dust? the gulf of California as a case study. *J. Geophys. Res. Oceans*. 125 (9), e2019JC015999. doi: 10.1029/2019JC015999
- Fishwick, M. P., Ussher, S. J., Sedwick, P. N., Lohan, M. C., Worsfold, P. J., Buck, K. N., et al. (2018). Impact of surface ocean conditions and aerosol provenance on the dissolution of aerosol manganese, cobalt, nickel and lead in seawater. *Mar. Chem.* 198, 28–43. doi: 10.1016/j.marchem.2017.11.003
- Frantoni, D. M., and Richardson, P. L. (2006). The evolution and demise of north Brazil current rings. *J. Phys. Oceanogr.* 36 (7), 1241–1264. doi: 10.1175/JPO2907.1
- Furey, H., Bower, A., Perez-Brunius, P., Hamilton, P., and Leben, R. (2018). Deep eddies in the gulf of Mexico observed with floats. *J. Phys. Oceanogr.* 48 (11), 2703–2719. doi: 10.1175/JPO-D-17-0245.1
- Gaube, P., Chelton, D. B., Strutton, P. G., and Behrenfeld, M. J. (2013). Satellite observations of chlorophyll, phytoplankton biomass, and Ekman pumping in nonlinear mesoscale eddies. *J. Geophys. Res. Oceans*. 118 (12), 6349–6370. doi: 10.1002/2013jc009027
- Glass, J. B., and Dupont, C. L. (2017). "Oceanic nickel biogeochemistry and the evolution of nickel use," in *The biological chemistry of nickel*. Eds. D. Zamble, M. Rowinska-Zyrek and H. Kozłowski (Croydon, UK: The Royal Society of Chemistry), 12–26.
- González-Ramírez, J., and Parés-Sierra, A. (2019). Streamflow modeling of five major rivers that flow into the gulf of Mexico using SWAT. *Atmosfera* 32, 261–272. doi: 10.20937/atm.2019.32.04.01
- Gordon, L. I., Jennings, J. C. Jr., Ross, A. A., and Krest, J. M. (1993). "A suggested protocol for continuous flow automated analysis of seawater nutrients (Phosphate, nitrate, nitrite and silicic acid) in the WOCE hydrographic program and the joint global ocean fluxes study," in *Technical report 93-1* (Corvallis, OR: Oregon State University).
- Hayes, C. T., Shiller, A. M., and Milroy, S. P. (2022). Toward constraining sources of lithogenic metals in the northern gulf of Mexico. *J. Geophys. Res. Oceans*. 127 (4), e2022JC018523. doi: 10.1029/2022JC018523
- Hayes, C. T., Wen, L. S., Lee, C. P., Santschi, P. H., and Johannesson, K. H. (2019). "Trace metals in the gulf of Mexico: Synthesis and future directions," in *Gulf of Mexico origin, waters and biota: Chemical oceanography*. Ed. T. S. Bianchi (College Station, TX: Texas A&M University Press), 93–119.
- Hernández-Candelario, I., d., C., Lares, M. L., Camacho-Ibar, V. F., Linacre, L., Gutiérrez-Mejía, E., et al. (2019). Dissolved cadmium and its relation to phosphate in the deep region of the gulf of Mexico. *J. Mar. Syst.* 193, 27–45. doi: 10.1016/j.jmarsys.2019.01.005
- Hernández-Sánchez, O. G., Camacho-Ibar, V. F., Fernández Álamo, M. A., and Herzka, S. Z. (2022). Nitrogen sources (NO<sub>3</sub>- vs N<sub>2</sub> fixation) inferred from bulk δ<sup>15</sup>N values of zooplankton from the deep water region of the gulf of Mexico. *J. Plankton. Res.* 44, 48–67. doi: 10.1093/plankt/fbab089
- Herut, B., Rahav, E., Tsagaraki, T. M., Giannakourou, A., Tsiola, A., Psarra, S., et al. (2016). The potential impact of saharan dust and polluted aerosols on microbial populations in the East Mediterranean Sea, an overview of a mesocosm experimental approach. *Front. Mar. Sci.* 3. doi: 10.3389/fmars.2016.00226
- Ho, T. Y. (2013). Nickel limitation of nitrogen fixation in trichodesmium. *Limnol. Oceanogr.* 58, 112–120. doi: 10.4319/lo.2013.58.1.0112
- Hollister, A. P., Kerr, M., Malki, K., Muhlbach, E., Robert, M., Tilney, C. L., et al. (2020). Regeneration of macronutrients and trace metals during phytoplankton decay: An experimental study. *Limnol. Oceanogr.* 65 (8), 1936–1960. doi: 10.1002/lno.11429
- Holl, C. M., Villareal, T. A., Payne, C. D., Clayton, T. D., Hart, C., and Montoya, J. P. (2007). *Trichodesmium* in the western gulf of Mexico: <sup>15</sup>N<sub>2</sub>-fixation and natural abundance stable isotopic evidence. *Limnol. Oceanogr.* 52 (5), 2249–2259. doi: 10.4319/lo.2007.52.5.2249
- Intergovernmental Oceanographic Commission [IOC], Scientific Committee on Oceanic Research [SCOR] and International Association for the Physical Sciences of the Oceans [IAPSO] (2010). *The international thermodynamic equation of seawater – 2010: Calculation and use of thermodynamic properties. intergovernmental oceanographic commission, manuals and guides no. 56* (Paris: UNESCO), 196.
- Jickells, T. D., Baker, A. R., and Chance, R. (2016). Atmospheric transport of trace elements and nutrients to the oceans. *Philos. Trans. R. Soc. A. Math. Phys. Eng. Sci.* 374, 20150286. doi: 10.1098/rsta.2015.0286
- Jickells, T. D., Dorling, S., Deuser, W. G., Church, T. M., Arimoto, R., and Prospero, J. M. (1998). Air-borne dust fluxes to a deep water sediment trap in the Sargasso Sea. *Global Biogeochem. Cycles*. 12 (2), 311–320. doi: 10.1029/97gb03368

- John, S. G., Kelly, R. L., Bian, X., Fu, F., Smith, M. I., Lanning, N. T., et al. (2022). The biogeochemical balance of oceanic nickel cycling. *Nat. Geosci.* 15, 906–912. doi: 10.1038/s41561-022-01045-7
- Joung, D., Guo, L., and Shiller, A. M. (2019). Role of the atchafalaya river basin in regulating export fluxes of dissolved organic carbon, nutrients, and trace elements to the Louisiana shelf. *J. Hydrol. X.* 2, 100018. doi: 10.1016/j.hydroa.2019.100018
- Joung, D., and Shiller, A. M. (2013). Trace element distributions in the water column near the deepwater horizon well blowout. *Environ. Sci. Technol.* 47 (5), 2161–2168. doi: 10.1021/es303167p
- Kantha, L. (2005). “Barotropic tides in the gulf of Mexico,” in *Circulation in the gulf of Mexico: Observations and models*. Eds. W. Sturges and A. Lugo-Fernandez (Washington, DC: AGU, Geophys. Monogr. Ser.), 159–163. doi: 10.1029/161GM13
- Komjarova, I., and Blust, R. (2006). Comparison of liquid-liquid extraction, solid-phase extraction and co-precipitation preconcentration methods for the determination of cadmium, copper, nickel, lead and zinc in seawater. *Anal. Chim. Acta* 576 (2), 221–228. doi: 10.1016/j.aca.2006.06.002
- Kremling, K. (1983). The behavior of zn, cd, Cu, Ni, Co, fe, and Mn in anoxic baltic waters. *Mar. Chem.* 13 (2), 87–108. doi: 10.1016/0304-4203(83)90019-1
- Kremling, K. (1985). The distribution of cadmium, copper, nickel, manganese, and aluminium in surface waters of the open Atlantic and European shelf area. *Deep Sea Res. Part A. Oceanogr. Res. Pap.* 32 (5), 531–555. doi: 10.1016/0198-0149(85)90043-3
- Kuznetsov, L., Toner, M., Kirwan, A. D., Jones, C. K. R. T., Kantha, L. H., and Choi, J. (2002). The loop current and adjacent rings delineated by Lagrangian analysis of the near-surface flow. *J. Mar. Res.* 60 (3), 405–429. doi: 10.1357/00224002762231151
- Lee-Sánchez, E., Camacho-Ibar, V. F., Velásquez-Aristizábal, J. A., Valencia-Gasti, J. A., and Samperio-Ramos, G. (2022). Impacts of mesoscale eddies on the nitrate distribution in the deep-water region of the gulf of Mexico. *J. Mar. Syst.* 229, 103721. doi: 10.1016/j.jmarsys.2022.103721
- Lemaitre, N., Du, J., de Souza, G. F., Archer, C., and Vance, D. (2022). The essential bioactive role of nickel in the oceans: Evidence from nickel isotopes. *earth planet. Sci. Lett.* 584, 117513. doi: 10.1016/j.epsl.2022.117513
- Lenes, J. M., Prospero, J. M., Landing, W. M., Virmani, J. I., and Walsh, J. J. (2012). A model of Saharan dust deposition to the eastern gulf of Mexico. *Mar. Chem.* 134, 1–9. doi: 10.1016/j.marchem.2012.02.007
- Lenstra, W. K., van Helmond, N. A. G. M., Zygadłowska, O. M., van Zummeren, R., Witbaard, R., and Slomp, C. P. (2022). Sediments as a source of iron, manganese, cobalt and nickel to continental shelf waters (Louisiana, gulf of Mexico). *Front. Mar. Sci.* 9. doi: 10.3389/fmars.2022.811953
- Lewis, B. L., and Landing, W. M. (1992). The investigation of dissolved and suspended particulate trace-metal fractionation in the black-Sea. *Mar. Chem.* 40 (1–2), 105–141. doi: 10.1016/0304-4203(92)90050-K
- Linacre, L., Durazo, R., Camacho-Ibar, V. F., Selph, K. E., Lara-Lara, J. R., Mirabal-Gómez, U., et al. (2019). Picoplankton carbon biomass assessments and distribution of prochlorococcus ecotypes linked to loop current eddies during summer in the southern gulf of Mexico. *J. Geophys. Res. Oceans.* 124 (11), 8342–8359. doi: 10.1029/2019JC015103
- Linacre, L., Lara-Lara, R., Camacho-Ibar, V., Herguera, J. C., Bazán-Guzmán, C., and Ferreira-Bartrina, V. (2015). Distribution pattern of picoplankton carbon biomass linked to mesoscale dynamics in the southern gulf of Mexico during winter conditions. *Deep Sea Res. Part I. Oceanogr. Res. Pap.* 106, 55–67. doi: 10.1016/j.dsr.2015.09.009
- Liu, T., Krisch, S., Xie, R. C., Hopwood, M. J., and Dengler, M. (2022). Sediment release in the benguela upwelling system dominates trace metal input to the shelf and Eastern south Atlantic ocean. *Global Biogeochem. Cycles.* 36 (9), e2022GB007466. doi: 10.1029/2022gb007466
- Mackey, D. J., O’Sullivan, J. E., Watson, R. J., and Dal Pont, G. (2002). Trace metals in the Western Pacific: Temporal and spatial variability in the concentrations of cd, Cu, Mn and Ni. *Deep Sea Res. Part I. Oceanogr. Res. Pap.* 49 (12), 2241–2259. doi: 10.1016/S0967-0637(02)00124-3
- Martínez-López, B., and Zavala-Hidalgo, J. (2009). Seasonal and interannual variability of cross-shelf transports of chlorophyll in the gulf of Mexico. *J. Mar. Syst.* 77 (1–2), 1–20. doi: 10.1016/j.jmarsys.2008.10.002
- Martin, A. P., and Richards, K. J. (2001). Mechanisms for vertical nutrient transport within a north Atlantic mesoscale eddy. *Deep Sea Res. Part II: Top. Stud. Oceanogr.* 48, 757–773. doi: 10.1016/S0967-0645(00)00096-5
- McGillcuddy, D. J. Jr. (2016). Mechanisms of physical-biological-biogeochemical interaction at the oceanic mesoscale. *Annu. Rev. Mar. Sci.* 8, 125–159. doi: 10.1146/annurev-marine-010814-015606
- Mellet, T., and Buck, K. N. (2020). Spatial and temporal variability of trace metals (Fe, Cu, Mn, zn, Co, Ni, cd, Pb), iron and copper speciation, and electroactive Fe-binding humic substances in surface waters of the eastern gulf of Mexico. *Mar. Chem.* 227, 103891. doi: 10.1016/j.marchem.2020.103891
- Meunier, T., Pallás-Sanz, E., Tenreiro, M., Portela, E., Ochoa, J., Ruiz-Angulo, A., et al. (2018). The vertical structure of a loop current eddy. *J. Geophys. Res. Oceans.* 123, 6070–6090. doi: 10.1029/2018JC013801
- Middag, R., de Baar, H. J. W., Bruland, K. W., and van Heuven, S. M. A. C. (2020). The distribution of nickel in the West-Atlantic ocean, its relationship with phosphate and a comparison to cadmium and zinc. *Front. Mar. Sci.* 7. doi: 10.3389/fmars.2020.00105
- Middag, R., Rolison, J. M., George, E., Gerringa, L. J. A., Rijkenberg, M. J. A., and Stirling, C. H. (2022). Basin scale distributions of dissolved manganese, nickel, zinc and cadmium in the Mediterranean Sea. *Mar. Chem.* 238, 104063. doi: 10.1016/j.marchem.2021.104063
- Morel, F. M. M., Milligan, A. J., and Saito, M. A. (2014). “8.5 - marine bioinorganic chemistry: The role of trace metals in the oceanic cycles of major nutrients,” in *Treatise on geochemistry (Second edition)*. Eds. H. D. Holland and K. K. Turekian (Oxford: Elsevier), 123–150. doi: 10.1016/B978-0-08-095975-7.00605-7
- Morley, N. H., Burton, J. D., Tankere, S. P. C., and Martin, J. M. (1997). Distribution and behaviour of some dissolved trace metals in the western Mediterranean Sea. *Deep Sea Res. Part II Top. Stud. Oceanogr.* 44, 675–691. doi: 10.1016/S0967-0645(96)00098-7
- Mulholland, M. R., Bernhardt, P. W., Heil, C. A., Bronk, D. A., and O’Neil, J. M. (2006). Nitrogen fixation and release of fixed nitrogen by trichodesmium spp. in the gulf of Mexico. *Limnol. Oceanogr.* 51, 1762–1776. doi: 10.4319/lo.2006.51.4.1762
- Oey, L., Ezer, T., and Lee, H. (2005). “Loop current, rings and related circulation in the gulf of Mexico: A review of numerical models and future challenges,” in *Circulation in the gulf of Mexico: Observations and model*. Eds. W. Sturges and A. Lugo-Fernandez (Washington, DC: AGU, Geophys. Monogr. Ser.), 31–56.
- Palenik, B., Brahamsha, B., Larimer, F. W., Land, M., Hauser, L., Chain, P., et al. (2003). The genome of a motile marine synechococcus. *Nature* 424, 1037–1042. doi: 10.1038/nature01943
- Pérez-Brunius, P., García-Carrillo, P., Dubrana, J., Sheinbaum, J., and Candela, J. (2013). Direct observations of the upper layer circulation in the southern gulf of Mexico. *Deep Sea Res. Part II: Top. Stud. Oceanogr.* 85, 182–194. doi: 10.1016/j.dsr2.2012.07.020
- Pinedo-Gonzalez, P., West, A. J., Tovar-Sánchez, A., Duarte, C. M., Marañón, E., Cermeño, P., et al. (2015). Surface distribution of dissolved trace metals in the oligotrophic ocean and their influence on phytoplankton biomass and productivity. *Global Biogeochem. Cycles.* 29 (10), 1763–1781. doi: 10.1002/2015GB005149
- Portela, E., Tenreiro, M., Pallás-Sanz, E., Meunier, T., Ruiz-Angulo, A., Sosa-Gutiérrez, R., et al. (2018). Hydrography of the central and western gulf of Mexico. *J. Geophys. Res. Oceans.* 123, 5134–5149. doi: 10.1029/2018JC013813
- Price, N. M., and Morel, F. M. M. (1991). Colimitation of phytoplankton growth by nickel and nitrogen. *Limnol. Oceanogr.* 36 (6), 1071–1077. doi: 10.4319/lo.1991.36.6.1071
- Saager, P. M., de Baar, H. J. W., de Jong, J. T. M., Nolting, R. F., and Schijf, J. (1997). Hydrography and local sources of dissolved trace metals Mn, Ni, Cu, and cd in the northeast Atlantic ocean. *Mar. Chem.* 57, 195–216. doi: 10.1016/S0304-4203(97)00038-8
- Saager, P. M., Schijf, J., and de Baar, H. J. W. (1993). Trace-metal distributions in seawater and anoxic brines in the Eastern Mediterranean-Sea. *Geochim. Cosmochim. Acta* 57 (7), 1419–1432. doi: 10.1016/0016-7037(93)90003-F
- Salas-de-León, D. A., Monreal-Gómez, M. A., Signoret, M., and Aldeco, J. (2004). Anticyclonic-cyclonic eddies and their impact on near-surface chlorophyll stocks and oxygen supersaturation over the campeche canyon, gulf of Mexico. *J. Geophys. Res. Oceans.* 109, C5. doi: 10.1029/2002jc001614
- Schlitzer, R. (2021) *Ocean data view*. Available at: <https://odv.awi.de> (Accessed September 1, 2021).
- Schlitzer, R., Anderson, R. F., Dodas, E. M., Lohan, M., Geibere, W., Tagliabue, A., et al. (2018). The GEOTRACES intermediate data product 2017. *Chem. Geol.* 493, 210–223. doi: 10.1016/J.CHEMGEO.2018.05.040
- Slater, F. R., Boyle, E., and Edmond, J. M. (1976). On the marine geochemistry of nickel. *earth planet. Sci. Lett.* 31, 119–128. doi: 10.1016/0012-821X(76)90103-5
- Sedwick, P. N., Bowie, A. R., Church, T. M., Cullen, J. T., Johnson, R. J., Lohan, M. C., et al. (2020). Dissolved iron in the Bermuda region of the subtropical north Atlantic ocean: Seasonal dynamics, mesoscale variability, and physicochemical speciation. *Mar. Chem.* 219, 103748. doi: 10.1016/j.marchem.2019.103748
- Segovia-Zavala, J. A., Lares, M. L., Delgado-Hinojosa, F., Tovar-Sánchez, A., and Sañudo-Wilhelmy, S. A. (2010). Dissolved iron distributions in the central region of the gulf of California, México. *Deep Sea Res. Part I. Oceanogr. Res. Pap.* 57, 53–64. doi: 10.1016/j.dsr.2009.10.007
- Seo, H., Kim, G., Kim, T., Kim, I., Ra, K., and Jeong, H. (2022). Trace elements (Fe, Mn, Co, Cu, cd, and Ni) in the East Sea (Japan sea): Distributions, boundary inputs, and scavenging processes. *Mar. Chem.* 239, 104070. doi: 10.1016/j.marchem.2021.104070
- Shelley, R. U., Sedwick, P. N., Bibby, T. S., Cabedo-Sanz, P., Church, T. M., Johnson, R. J., et al. (2012). Controls on dissolved cobalt in surface waters of the Sargasso Sea: Comparisons with iron and aluminum. *Global Biogeochem. Cycles* 26, GB2020. doi: 10.1029/2011GB004155

- Sosa-Gutiérrez, R., Pallàs-Sanz, E., Jouanno, J., Chaigneau, A., Candela, J., and Tenreiro, M. (2020). Erosion of the subsurface salinity maximum of the loop current eddies from glider observations and a numerical model. *J. Geophys. Res. Oceans*. 125, e2019JC015397. doi: 10.1029/2019JC015397
- Sunda, W. G. (1989). Trace metal interactions with marine phytoplankton. *Biol. Oceanogr.* 6, 411–442. doi: 10.1080/01965581.1988.10749543
- Tomczak, M., and Godfrey, J. S. (2003). *Regional oceanography: An introduction* (Oxford: Elsevier).
- Tovar-Sánchez, A. (2012). “Sampling approaches for trace elements determination in seawater,” in *Comprehensive sampling and sample preparation*. Ed. J. Pawliszyn (Oxford: Academic Press), 317–334. doi: 10.1016/B978-0-12-381373-2.00017-X
- Tovar-Sánchez, A., and Sañudo-Wilhelmy, S. A. (2011). Influence of the Amazon river on dissolved and intra-cellular metal concentrations in trichodesmium colonies along the western boundary of the sub-tropical north Atlantic ocean. *Biogeosciences* 8, 217–225. doi: 10.5194/bg-8-217-2011
- Tovar-Sánchez, A., Sañudo-Wilhelmy, S. A., Kustka, A. B., Agustí, S., Dachs, J., Hutchins, D. A., et al. (2006). Effects of dust deposition and river discharges on trace metal composition of trichodesmium spp. in the tropical and subtropical north Atlantic ocean. *Limnol. Oceanogr.* 51, 1755–1761. doi: 10.4319/lo.2006.51.4.1755
- Turner, R. E., and Rabalais, N. N. (2019). “The gulf of Mexico,” in *World seas: An environmental evaluation: Volume I: Europe, the Americas and West Africa*. Ed. C. Sheppard (Cambridge: Academic Press), 445–464.
- Twining, B., Baines, S., Vogt, S. B., and Nelson, D. M. (2012). Role of diatoms in nickel biogeochemistry in the ocean. *Global Biogeochem. Cycles* 26, 1–9. doi: 10.1029/2011gb004233
- Valencia-Gasti, J. A., Camacho-Ibar, V. F., and Herguera, J. C. (2022). Water mass structure and mixing fractions in the deepwater region of the gulf of Mexico. *J. Geophys. Res. Oceans*. 127, e2021JC017705. doi: 10.1029/2021jc017705
- Vázquez de la Cerda, A. M., Reid, R. O., DiMarco, S. F., and Jochens, A. E. (2005). “Bay of Campeche circulation: An update,” in *Circulation in the Gulf of Mexico: Observations and models*. Eds. W. Sturges and A. Lugo-Fernandez (Washington, DC: AGU, Geophys. Monogr. Ser.), 279–293.
- Velásquez-Aristizábal, J. A., Camacho-Ibar, V. F., Durazo, R., Valencia-Gasti, J. A., Lee-Sánchez, E., and Traviña-Castro, A. (2022). Nitrate/Hydrographic classification and prediction of nitrate profiles for oceanographic stations under the influence of mesoscale eddies in the Gulf of Mexico. *Front. Mar. Sci.* 9. doi: 10.3389/fmars.2022.827574
- Wen, L.-S., Jiann, K.-T., and Santschi, P. H. (2006). Physicochemical speciation of bioactive trace metals (Cd, Cu, Fe, Ni) in the oligotrophic south China Sea. *Mar. Chem.* 101, 104–129. doi: 10.1016/j.marchem.2006.01.005
- Wen, L.-S., Santschi, P. H., Warnken, K. W., Davison, W., Zhang, H., Li, H. P., et al. (2011). Molecular weight and chemical reactivity of dissolved trace metals (Cd, Cu, Ni) in surface waters from the Mississippi river to Gulf of Mexico. *Estuar. Coast. Shelf. Sci.* 92, 649–658. doi: 10.1016/j.ecss.2011.03.009
- Yeats, P. A., and Campbell, J. A. (1983). Nickel, copper, cadmium and zinc in the northwest Atlantic ocean. *Mar. Chem.* 12 (1), 43–58. doi: 10.1016/0304-4203(83)90027-0
- Yeats, P. A., Westerlund, S., and Flegel, A. R. (1995). Cadmium, copper and nickel distributions at four stations in the eastern central and south Atlantic. *Mar. Chem.* 49 (4), 283–293. doi: 10.1016/0304-4203(95)00018-M
- Zeri, C., and Voutsinou-Taliadouri, F. (2003). Processes affecting the distribution of dissolved trace metals in the north Aegean Sea (Eastern Mediterranean). *Cont. Shelf. Res.* 23 (9), 919–934. doi: 10.1016/s0278-4343(03)00022-0
- Zhang, R., Ren, J., Zhang, Z., Zhu, Z., and John, S. (2022). Distribution patterns of dissolved trace metals (Fe, Ni, Cu, Zn, Cd, and Pb) in China marginal seas during the GEOTRACES GP06-CN cruise. *Chem. Geol.* 604, 120948. doi: 10.1016/j.chemgeo.2022.120948